Contract Nonr 839(38)

A CRITICAL ANALYSIS OF NUMERICAL TECHNIQUES: THE PISTON-DRIVEN INVISCID FLOW

by

Gino Moretti

JULY 1969

POLYTECHNIC INSTITUTE OF BROOKLYN

DEPARTMENT
of
AEROSPACE ENGINEERING
and
APPLIED MECHANICS

PIBAL REPORT 69-25

A CRITICAL ANALYSIS OF NUMERICAL TECHNIQUES: THE PISTON-DRIVEN INVISCID FLOW

by

Gino Moretti

This research has been conducted under Contract Nonr 839(38) for PROJECT STRATEGIC TECHNOLOGY and was made possible by the support of the Advanced Research Projects Agency under Order No. 529 through the Office of Naval Research.

Polytechnic Institute of Brooklyn

Department

of

Aerospace Engineering and Applied Mechanics

July 1969

PIBAL REPORT NO. 69-25

BLANK PAGE

Table of Contents

A CRITICAL ANALYSIS OF NUMERICAL TECHNIQUES: THE PISTON-DRIVEN INVISCID FLOW [+]

by

Gino Moretti[*]
Polytechnic Institute of Brooklyn
Graduate Center, Farmingdale, New York

ABSTRACT

This paper consists of two parts. In the first, a critical analysis of well-known procedures for the computation of one-dimensional shocked flows is made, in order to show the inconveniences of computing finite differences across a discontinuity and to prove that the use of the equations of motion in conservation form does not make the results any more accurate. In the second, a technique is developed to treat one-dimensional inviscid problems and it is applied to the problem of an accelerating piston. Practical and safe ways to predict the formation of a shock and to follow it up in its evolution are given.

[+] This research has been conducted under Contract No. Nonr 839(38) for PROJECT STRATEGIC TECHNOLOGY and was made possible by the support of the Advanced Research Projects Agency under Order No. 529 through the Office of Naval Research.

[*] Professor of Aerospace Engineering.

Introduction

The numerical treatment of one-dimensional problems has been the object of a great number of papers, mostly intended to provide theoretical and experimental comparisons between different numerical techniques. Such comparisons have failed to provide a positive contribution to the state of the art. They have been unable, for example, to point out why the results of the computations are generally affected by spurious oscillations, and why their accuracy is so poor, although some qualitative agreement with exact solutions, when available, can be observed.

In Ref. 1 a general line of attack for gas dynamics problems has been presented, the philosophy of which is that computations can be performed in any number of space dimensions and time with as great an accuracy as desired. Such a goal can be achieved not only without increasing the computational time beyond unacceptable limits but rather reducing it by at least one order of magnitude.

A test of the technique outlined in Ref. 1 is given here for one-dimensional problems. A detailed analysis of some of these problems is necessary in order to explain the physical subtlety of certain non-linear phenomena and of their interpretation from the view point of numerical analysis.

In the first part of the paper, the problem of a steady shock separating two regions of uniform flow is examined in an attempt to explain the origin of certain well-known numerical difficulties. In the second and third parts, an increasingly sophisticated technique is introduced, to show how such difficulties can be, one by one, eliminated. A demonstration of how the technique can be applied to very complicated one-dimensional inviscid problems will follow in another paper.

1. Shocks and the equations in divergence form

In the typical one-dimensional problem analyzed in the literature, a shock proceeds, at a constant speed, into a gas at rest. The region behind the shock is, then, uniform. The flow pattern can be imagined to be produced by a piston suddenly set into motion at a constant speed (Fig. 1). The shock is not assumed to be a discontinuity; the numerical techniques intend to provide a way of representing the shock as a fast, but continuous, transition between two constant states.

If the approach outlined in Ref. 1 were used for this problem, the flow field would be divided into two regions of continuous flow and the shock confined to the common boundary. Then the problem becomes trivial; in both regions separated by the shock the flow is uniform, all space derivatives vanish identically and consequently the time derivatives vanish identically. There is no doubt that, regardless of the technique

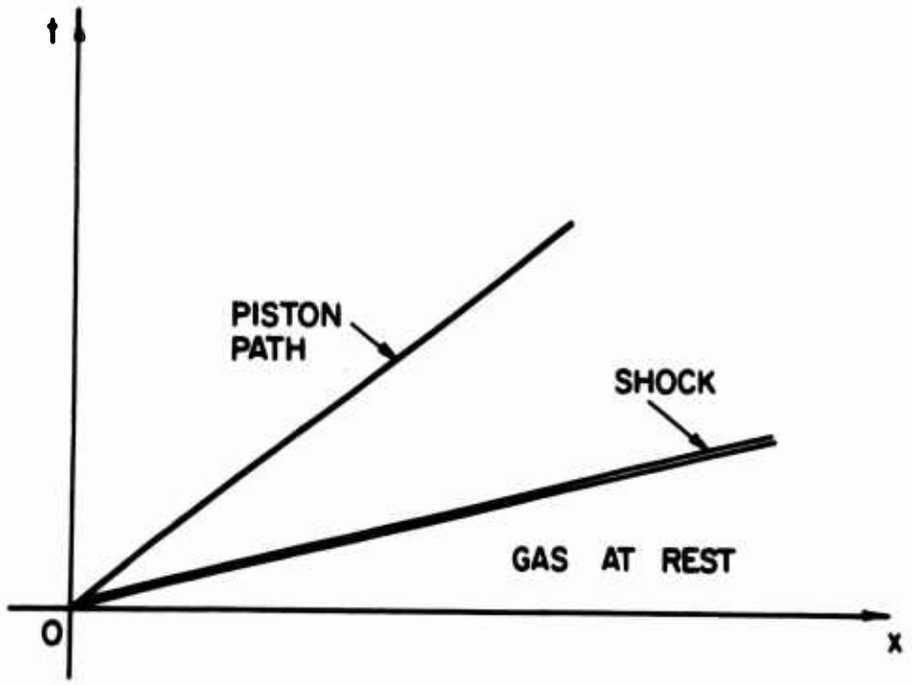

FIG. 1 FLOW PRODUCED BY A PISTON MOVING AT A CONSTANT SPEED

being used, the two constant states are maintained. As far as the shock itself is concerned, a single application of the Rankine-Hugoniot conditions provides the solution at any instant of time since the shock velocity is constant. In the first part of this paper, however, we will re-examine the simple flow problem outlined in Fig. 1 to discuss the basic philosophy of the "smeared shock" approach and to justify our choice of the other approach as outlined in Ref. 1.

There is no doubt that if one could handle shocks by the same technique used in regions of continuous flow, the general logic of a computational program would be highly simplified, particularly when a flow is expected to be traversed by shocks in both directions and when the problem depends on more than one space variable. However, anyone who has some experience in computing by the method of characteristics knows that, as soon as the characteristics coalesce and a shock builds up, the method breaks down. The only way the computation can be continued consists of fitting the shock as a discontinuity, separating two regions of continuous flow where the method of characteristics is applicable. The physical nature of the shock is reflected in the numerical procedure by the fact that each shock point is reached by three characteristics, two in the supersonic region and one in the subsonic region, plus the particle path in the supersonic region (Fig. 2) (the Mach numbers being computed from the velocities relative to the shock). Therefore, if one pretends to ignore the shock, one is forced to face a redundancy of data which are inconsistent as long as no jump is permitted.

It is rather surprising that so much effort has been spent against

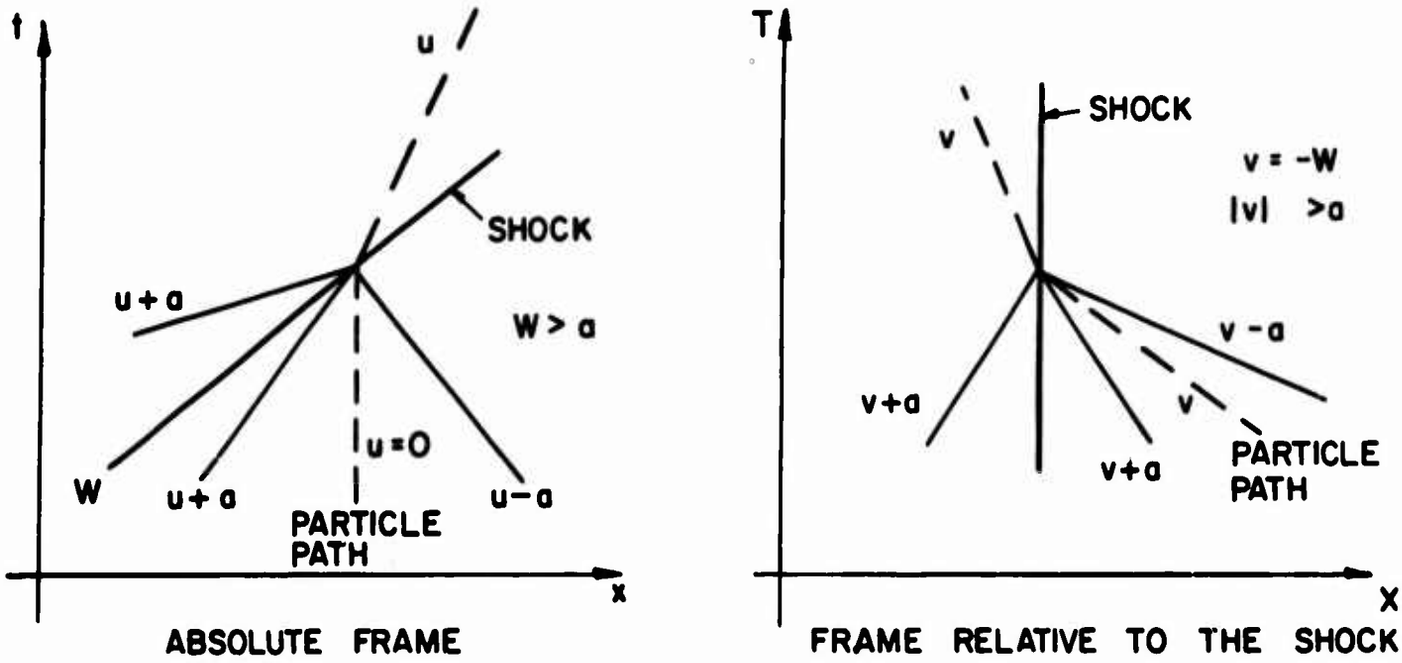

FIG. 2 CHARACTERISTIC PATTERN ON BOTH SIDES OF A SHOCK

the evidence offered by the method of characteristics and even against a basic principle of mathematics, as we will see later on. There is apparently only one possible explanation, which we will try to present here, as plainly as possible.

1.1 The smearing out of a shock according to von Neumann and Richtmyer.

Let us consider the problem in its historical development. In 1950, von Neumann and Richtmyer, trying to solve the problem of shocked flows by numerical techniques, found the amount of labor involved too great, even using automatic computers (in 1950, programming for a machine like ENIAC was extremely cumbersome; FORTRAN was invented many years later). Von Neumann and Richtmyer had in mind multidimensional shocked flows. A treatment similar to the one outlined in Ref. 1 was, at that time, beyond reach, as they stated: "Shock calculations by direct application of the Hugoniot equations would ordinarily be prohibitively difficult, even for rapid, automatic computers." (Ref. 2) Consequently, they suggested a device, inspired

by the physical behavior of a gas crossing a shock. When viscosity and heat conduction are taken into account, shocks are naturally smeared out and can be described as a continuous transition. The larger the viscous effects, the wider the transitional region. It is known that, except when the gas is rarefied, this region is still too thin to be perceivable. However, von Neumann and Richtmyer thought that an artificial viscosity could be forced into the equations of motion in such a way that (i) the shock transition would be spread out over, say, a couple of mesh intervals (which meant to have an unrealistically large viscosity in that region), but also (ii) managing to keep the viscous effects negligible in the rest of the computational mesh. The suggested artificial viscosity for one-dimensional problems depended on a term containing u_x^2.

The aim of the suggested device is to compute inviscid flows with numerical methods apt to approximate continuous flows, without having to make special provisions for shocks in advance, but reaching a good approximation to the inviscid flow solution, except on a two mesh interval bracketing each shock.

1.2 Lax's technique: artificial viscosity and the equations in conservation form.

In 1954, Lax (Ref. 3) suggested two modifications to the above approach. The first had to do with a way of introducing artificial viscosity. To see the idea without complications, consider the equation

$$f_t = g_x \tag{1}$$

Let the points to be computed (nodal points) be equally spaced along the x-axis, so that their abscissae are $x_n = n\Delta x$ ($n = 1, 2, 3, \ldots$). Let k denote a value of time $t_k = k\Delta t$. Let f_n^k denote the value of f at $x = x_n$ and $t = t_k$. Approximate g_x by centered differences $(g_{n+1}^k - g_{n-1}^k)/2\,\Delta x$

but, instead of writing

$$f_n^{k+1} = f_n^k + \frac{g_{n+1}^k - g_{n-1}^k}{2\Delta x} \tag{2}$$

as one would do by a straight forward application of Euler's integration rule, let us write

$$f_n^{k+1} = \frac{f_{n+1}^k + f_{n-1}^k}{2} + \frac{g_{n+1}^k - g_{n-1}^k}{2\ \Delta x}\ \Delta t \tag{3}$$

In other words, the initial value of f used to approximate the time derivative at the n-th point is not the value of f at the n-th point but the <u>average</u> of the values of f at the two neighboring points.

On the other hand, if we consider the equation

$$f_t = g_x + \nu f_{xx} \tag{4}$$

with

$$\nu = \frac{\Delta x^2}{2\Delta t} \tag{5}$$

approximate f_{xx} by $(f_{n+1}^k + f_{n-1}^k - 2 f_n^k) / \Delta x^2$, and use an integration scheme similar to (2), we obtain (3) again. Terms containing second order spatial derivatives, such as νf_{xx}, appear in the Navier-Stokes equations, where ν is proportional to the kinematic viscosity of the gas (in non-dimensional form, ν is the inverse of a Reynolds number). Therefore, we may consider (3) as a formula solving a problem of motion, somehow affected by a pseudo-viscosity whose Reynolds number is of the order of $1/\nu$.

The second innovation in Lax's technique consisted of approximating by a finite-difference scheme not the well-known Euler's equations

$$\begin{cases} \rho_t + u\rho_x + \rho u_x = 0 \\ \rho u_t + \rho u u_x + p_x = 0 \\ S_t + u S_x = 0 \end{cases} \tag{6}$$

but a system written in what is called a <u>divergence form</u>, or <u>conservation form</u>.

Such a system can be obtained by algebraic manipulation of (6) or directly from the equations expressing conservation of mass, momentum and energy. Let

$$m = \rho u \tag{7}$$

$$E = \frac{1}{\gamma-1}\, p + \frac{1}{2}\rho u^2 = \frac{1}{\gamma-1}\, p + \frac{1}{2}\,\frac{m^2}{\rho} \tag{8}$$

$$H = u\left(\frac{\gamma}{\gamma-1}\, p + \frac{1}{2}\,\rho u^2\right) = \frac{m}{\rho}\left(\gamma E - \frac{\gamma-1}{2}\,\frac{m^2}{\rho}\right) \tag{9}$$

$$q = p + \rho u^2 = (\gamma-1)\, E + \frac{3-\gamma}{2}\,\frac{m^2}{\rho} \tag{10}$$

The conservation equations mentioned above can be written in the form:

$$\begin{cases} \rho_t = - m_x \\ m_t = - q_x \\ E_t = - H_x \end{cases} \tag{11}$$

and it is easy to see that (11) is equivalent to (6). Formally, the system consists now of linear relations between first derivatives. The system, however, is obviously non linear since the dependent variables are related to one another by the non linear equations (7), (9), and (10).

Note that (1) may represent all three equations of motion if f and g are considered as vectors, defined by

$$f = \begin{bmatrix} \rho \\ m \\ E \end{bmatrix} \quad , \quad g = - \begin{bmatrix} m \\ q \\ H \end{bmatrix} \tag{12}$$

What happens if the motion is steady is remarkable (and, incidentally, the arguments and conclusions which follow are not limited to one-dimensional

problems). The left-hand sides of the equations vanish identically. Therefore, the same is true of the right-hand sides. And, of course, the statement holds wherever the original equations (11) are applicable, that is, throughout all region where the flow parameters are continuous and differentiable. On the other hand, consider the Rankine-Hugoniot conditions across a shock,

$$\begin{aligned} \rho_1 v_1 &= \rho_2 v_2 \\ \rho_1 v_1^2 + p_1 &= \rho_2 v_2^2 + p_2 \\ h_1 + \frac{1}{2} v_1^2 &= h_2 + \frac{1}{2} v_2^2 \end{aligned} \tag{13}$$

where v is the velocity relative to the shock, h is the enthalpy:

$$h = \frac{\gamma}{\gamma-1} \frac{p}{\rho} \tag{14}$$

and the subscripts 1 and 2 refer to conditions on either side of the shock. In a steady state, the velocity v coincides with u. By using the definitions (7), (10) and (9), the Rankine-Hugoniot conditions can be written as

$$\begin{aligned} m_1 &= m_2 \\ q_1 &= q_2 \\ H_1 &= H_2 \end{aligned} \tag{15}$$

In other words, the quantities m, q, and H (in physical terms, mass flow, momentum and total enthalpy) are <u>continuous</u> across a shock. And since $m_x \equiv 0$, $q_x \equiv 0$, $H_x \equiv 0$ everywhere else, m, q, and H are constant throughout the flow. It is obvious, then, that any finite-difference approximation to the x-derivatives of m, q, and H vanishes identically, <u>even if the nodes lie at opposite sides of a shock</u>. By using the equations in the form (11) their finite-difference counterparts can be used all throughout a shocked flow even when the individual components of mass, momentum and total enthalpy,

that is, density, velocity and pressure, are not continuous (and thus not differentiable) across a shock. Let us hasten to say that a statement of this kind, although obviously true, is a deceiving one. What it actually means is that if we compute a steady flow by finite-difference technique as if it were unsteady, and we use as initial conditions the correct steady flow, and we use the equations in conversation form, we find that all time derivatives are zero, and therefore we compute nothing at all. The result is self-consistent but is trivial.

It is surely a better result than what we would have got, had we used a finite difference counterpart to (6) in the presence of a shock since finite-difference approximations to the space derivatives across a steady shock would generally provide finite values of the time derivatives, and therefore local changes in the physical parameters, a result which is inconsistent with the steady state assumption.

The question is, Does then a set of finite-difference equations obtained from (11) give better results than a set obtained from (6) when the flow is not steady? Lax himself did not attempt to prove anything of the sort; he only advanced some hopeful conjectures. Then he made some numerical work to try out his innovations. Fig. 3 is a plot of the pressure distribution as described in Table V of Lax's paper, (Ref. 3). The theoretical distribution is a constant line, at $p = 50$, followed by a constant line at $p = 0$. The transition should occur approximately where indicated. The figure shows a typical "qualitatively good" result. Let us analyze it, however, keeping in mind that two questions must be answered, viz.

(i) Is the transition replacing the shock sufficiently sharp?, and (ii) Does the conservation form of the equations solve the problem of computing across a shock?

Two features of the figure should be considered carefully. The

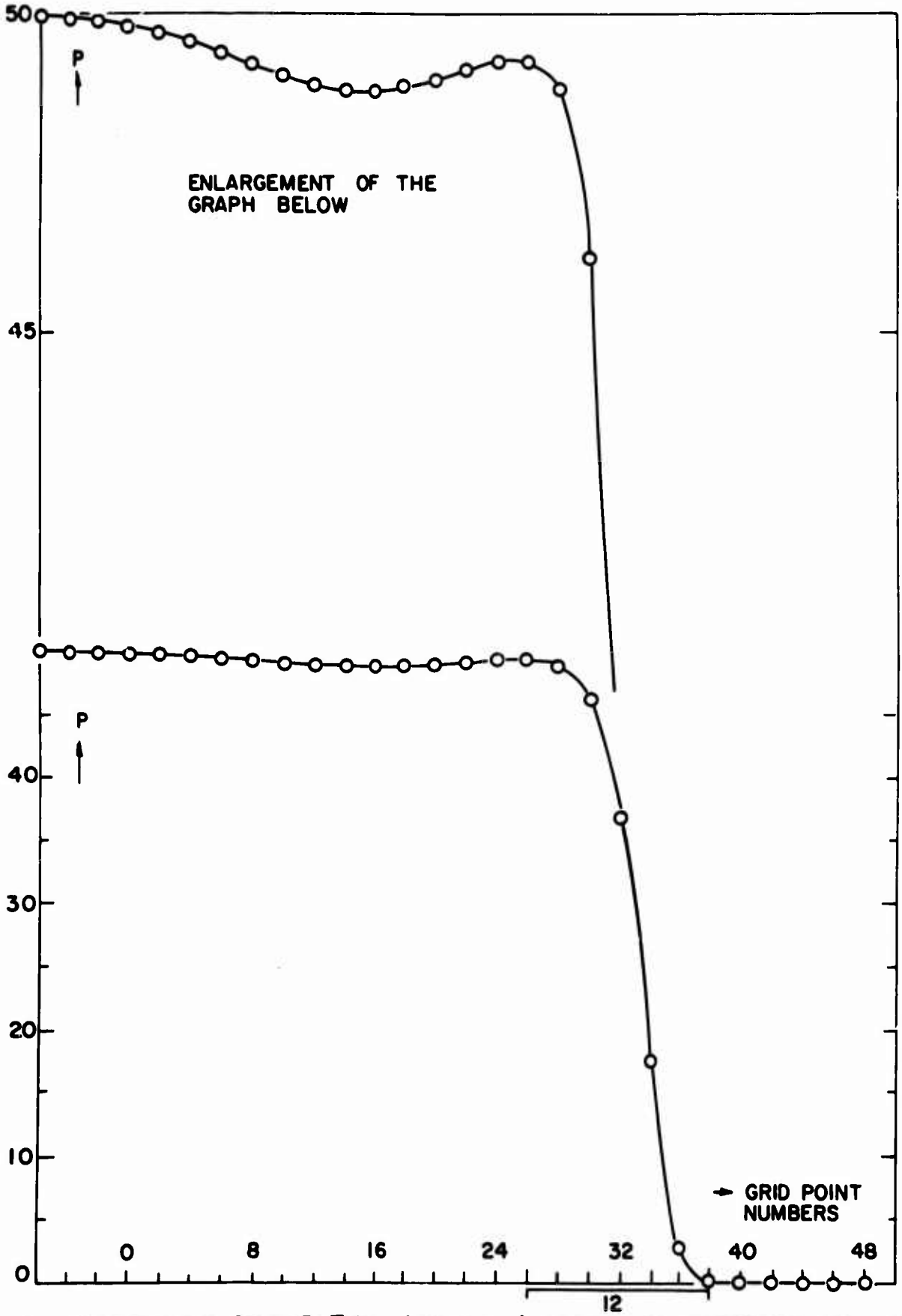

FIG. 3 PRESSURE DISTRIBUTION ACROSS A SHOCK, AS COMPUTED BY LAX

first is the number of mesh intervals along which the shock is spread. The second is a mild oscillation appearing in the high pressure side of the "shock" (to make it more evident, part of the plot has been redrawn at a larger scale in the upper part of the figure). These two features are typical of numerical effects which are unrelatable to the physical nature of the flow. We are going to discuss them in detail in the first part of this paper, showing that the oscillation is the typical symptom of numerical trouble in attempting to deal with a discontinuity by "continuous" techniques, whereas the spreading of the transition over too many mesh points is the telltale of a gigantic artificial viscosity.

Unfortunately, in Lax's procedure one effect cannot be studied without having the other as well, and conclusions cannot be easily drawn.* However, one can grasp the idea by comparing Figs. 3 and 4 where some results obtained by Emery (Ref. 4) with the Lax scheme are replotted. The curve at the left and the one at the right of Fig. 4 were obtained by using $\Delta t/\Delta x = .9$ and $\Delta t/\Delta x = .7$, respectively. The curve of Fig. 3 corresponds to $\Delta t/\Delta x = .25$. In a real shock, for a given Mach number (not much higher than 4), the shock thickness δ is roughly proportional to the inverse of the Reynolds number. In Lax's scheme,(5) shows that the Reynolds number is proportional to $\Delta t/\Delta x^2$. Therefore, the product $\delta(\Delta t/\Delta x^2)$ should be practically the same for all three cases if the artificial viscosity acts as a real viscosity. Now, $\delta/\Delta x$ is the number of intervals over which the "shock" is spread.

---

* This is due to the fact that the Euler's integration rule (2) is unconditionally unstable and (3), as we have seen, contains artificial viscosity.

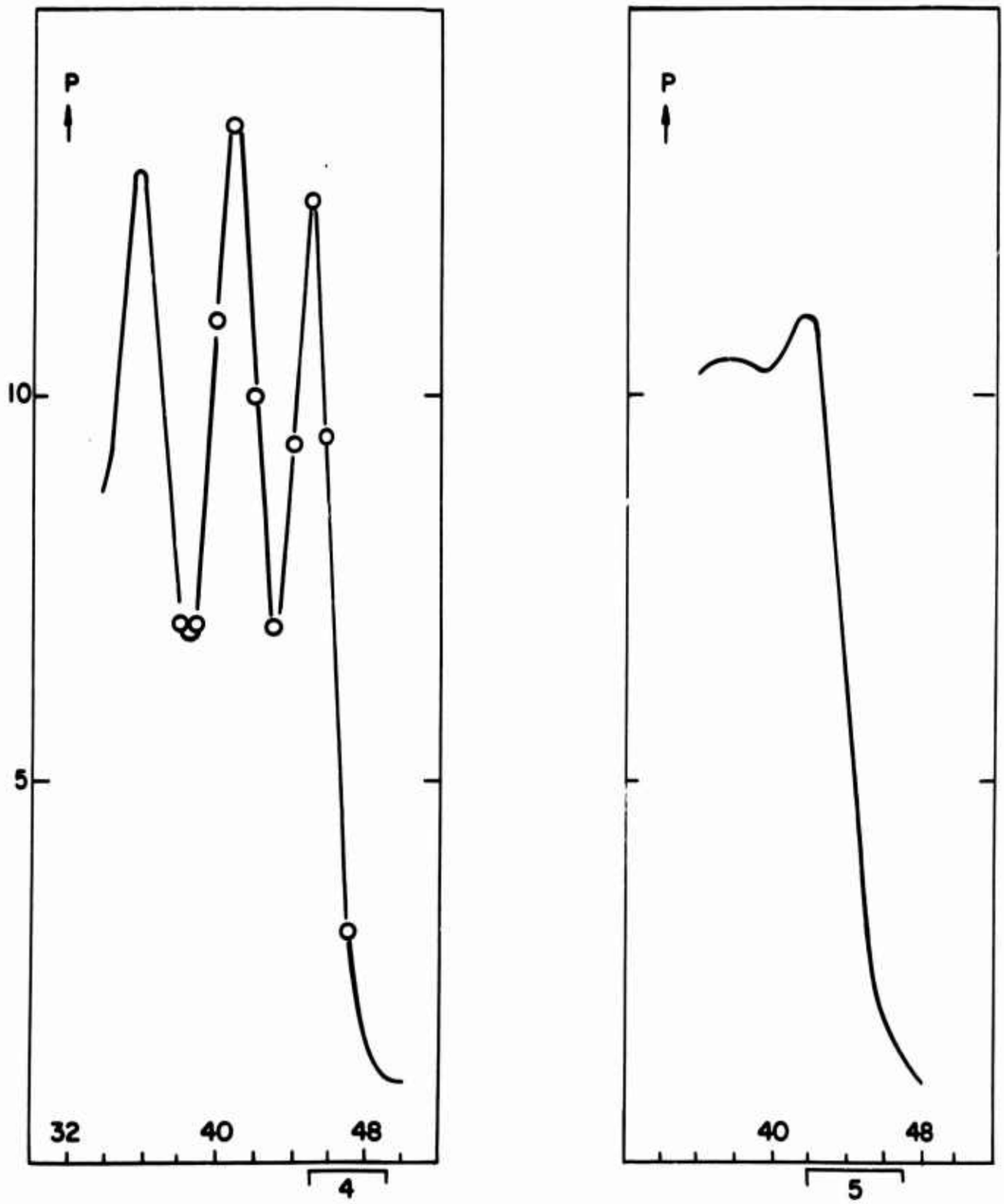

FIG. 4 PRESSURE DISTRIBUTION ACROSS A SHOCK, AS COMPUTED BY EMERY, USING LAX'S SCHEME

From the figures we find

$\delta/\Delta x$	$\Delta t/\Delta x$	$\delta(\Delta t/\Delta x^2)$
12	.25	3
5	.7	3.5
4	.9	3.6

From the figures of the last column we can conclude that the effects of artificial viscosity on shock thickness are very similar to the effects of real viscosity. Unfortunately, we can also see that the artificial Reynolds number per unit length is of the order of $1/\Delta x$. In practice one deals with intervals which cannot be smaller than, say, 1/50 of a typical reference length, lest the computational time increases beyond acceptable limits. Therefore the artificial Reynolds number is, at most, of the order of 50.

Figs. 3 and 4 show that the artificial viscosity plays a crucial role in damping out the oscillations and that an effective damping is obtained only if the artificial Reynolds number is extremely low, so that the transition replacing the shock cannot be sufficiently sharp.

1.3. The Lax-Wendroff Technique.

Reducing the artificial viscosity in Lax's scheme entails increasing the amplitude of the oscillations in the high-pressure side of the shock. Therefore we cannot evaluate whether the conservation form of the equation of motion is of any help in computing a flow which contains a sharp discontinuity. For such an analysis, one needs a scheme which can work in the absence of artificial viscosity. The scheme suggested by Lax and Wendroff in 1960 (Ref. 5) seems to be aimed at increasing the accuracy, and eliminating artificial viscosity, while maintaining the formulation of the equations in conservation form, obviously in the hope that shocked flows could be treated without shock fitting.

The Lax-Wendroff scheme, in principle, depends on approximating the unknowns at a time $t + \Delta t$ by a Taylor expansion truncated at the second order terms:

$$f(t + \Delta t) = f(t) + f_t \Delta t + \frac{1}{2} f_{tt} \Delta t^2 \tag{16}$$

expressing the time derivatives through space derivatives, making use of the equations of motion, and replacing the space derivatives by centered differences. Lax and Wendroff have applied the scheme to the equations of motion formulated in conservation form. In the one-dimensional case, (11) is the starting point. Then (16) is used. To compute f_{tt}, (1) is differentiated with respect to t:

$$f_{tt} = g_{tx}$$

but

$$g_t = J f_t = J g_x$$

(where J is the matrix whose determinant is the Jacobian of g with respect to f), so that

$$f_{tt} = (J g_x)_x \tag{17}$$

For no apparent reason, $(J g_x)_x$ is not resolved into

$$(J g_x)_x = J_x g_x + J g_{xx} \tag{18}$$

but is computed as

$$(J g_x)_x = \left(\frac{J^k_{n+1} + J^k_n}{2} \frac{g^k_{n+1} - g^k_n}{\Delta x} - \frac{J^k_n + J^k_{n-1}}{2} \frac{g^k_n - g^k_{n-1}}{\Delta x} \right) \frac{1}{\Delta x} \tag{19}$$

which implies an averaging of J and, thus, a higher truncation error than if (18) were used.

We would like to mention in passing that the scheme suggested by (16) does not require the equations of motion to be cast in conservation form. From a practical point of view, it is more convenient to use Euler's

equations. Recasting the equations of motion in conservation form is a cumbersome process, particularly when more than one space dimension is involved. Auxiliary mappings of the physical space onto a computational space make the procedure even more complicated, if not impossible. The Jacobian matrices in multi-dimensional problems not only are complicated but require a great amount of numerical computations which is avoided if Euler's equations are used. In conclusion, a program based on the original Lax-Wendroff suggestion is more complicated (and consequently more exposed to accidental mistakes), much more time consuming on the machine and less accurate than a program applying (16) to Euler's equations.

Of course, these disadvantages would be largely balanced by the possibility of treating shocks as sharp transitions. However, the equations in conservation form do not keep up to the hopes suggested by Lax's conjectures. Fig. 5 shows a typical result obtained by Lax and Wendroff. Here the oscillations in the high-pressure side of the shock are much stronger than in Fig. 1. The figure is borrowed from page 333 of Richtmyer and

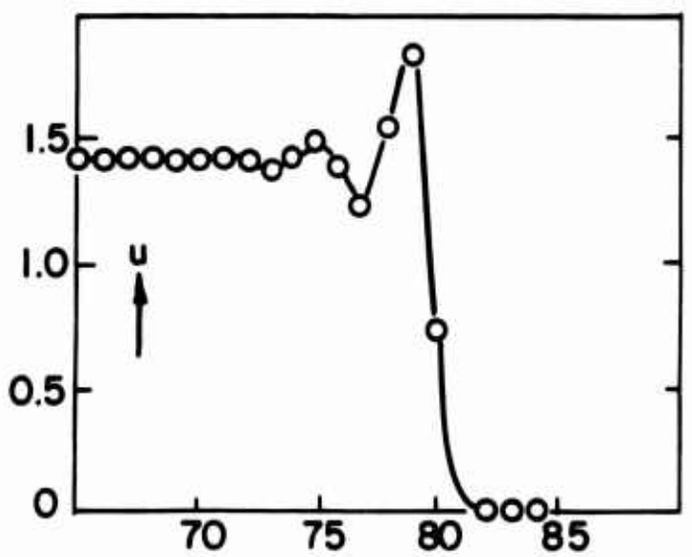

FIG. 5 VELOCITY DISTRIBUTION ACROSS A SHOCK, AS COMPUTED BY LAX AND WENDROFF

Morton's book (Ref. 6), where no explanation is given for the appearance of the oscillations. It is only stated that the oscillations can be reduced by adding again an artificial viscosity to the equation of motion.

1.4 Explaining the formation of wiggles.

From the examples above it appears that wiggles tend to form in the high-pressure side of a shock, regardless of the computational technique being used, unless artificial damping devices are used. Here we attempt to explain the formation of such wiggles. We are interested, of course, in a numerical scheme whose artificial viscosity, if any, is such that the shock is not spread over more than one mesh interval. We consider a shock moving from left to right at a constant speed, W, and separating two regions of uniform flow. Consider three points, labeled n-1, n, and n+1 at the abscissae $x-\Delta x$, x, and $x+\Delta x$ (Fig. 6) and suppose that, when a certain computation is started, the shock is somewhere between $x-\Delta x$ and x. Even if we are willing to accept a continuous transition instead of the jump at the shock, we must acknowledge that the numerical scheme is

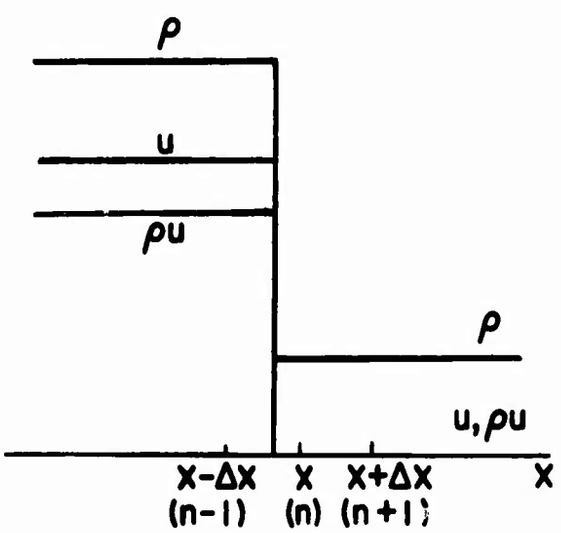

FIG. 6 DISCONTINUITIES ACROSS A SHOCK

unable to distinguish between such a transition and a jump, since both take place between two adjacent nodes and the values of the physical parameters are defined only at nodes. Under these conditions, we can show how oscillations build up long before a steady state, when physically existing, can be reached.

In the above problem, the three quantities m, q, and H are higher at the left of the shock than at the right*. The same may be said of ρ, p, u, and E. Let F be any of these quantities and let Fig. 7a represent what the F-distribution should actually be at a certain time t. In the same figure, a set of initial values for a numerical computation is also shown, at a discreet number of nodal points. At all nodal points except A and B the results of a numerical computation are correct. We are going to analyze the results of one computational step at points A and B by assuming that

$$\left|\frac{1}{2} f_{tt} \Delta t^2\right| < \left|f_t \Delta t\right| \quad . \tag{20}$$

Such a condition can always be satisfied if Δt is chosen sufficiently small. Note then that the numerical approximations to the derivatives at A and B, as shown in Fig. 7b by the dotted lines, are negative; according to (11), all quantities F increase at A and B. At $t + \Delta t$, the actual F-distribution (where the shock moved somewhat ahead) and the computed F-distribution are as in Fig. 7c. Now points C and D start being affected by errors and we analyze the results of a second computational step with (20) still valid. The approximate derivatives are negative at A, B and D, and positive at C; consequently F increases at A, B and D and decreases at C (Fig. 7d.) Without pursuing the argument any further, one can already see the

---

* They are the same only if the shock is steady.

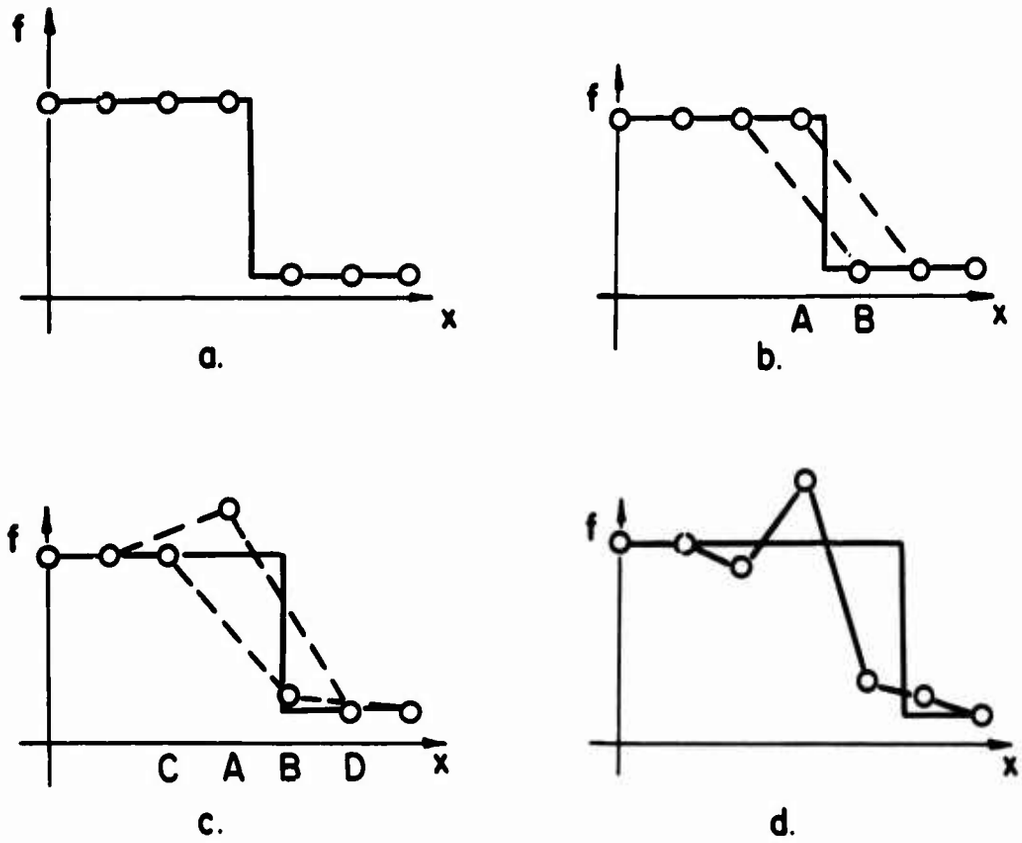

FIG. 7 FORMATION OF WIGGLES

formation of a wiggle on the high pressure side of the shock. This is a common, typical situation, due to a bold, but hardly justifiable, attempt to compute derivatives across a discontinuity; and it is a first-order effect. The introduction of higher order terms, as in the Lax-Wendroff technique, is irrelevant as far as this effect is concerned.

However, as the computation proceeds, the second order terms in (16) become more and more important and they are finally responsible for the partially oscillatory and unsymmetrical distributions typified by Fig. 5. A simple example is offered by the density distribution, which is governed by the first of (11). The second order term in the finite-difference formulation has the sign of m_{xx} and it grows with m_{xx}. As the amplitude of the

oscillations increases, the contribution of $\frac{1}{2} m_{xx} \Delta t^2$ ends by becoming of the same order as $m_x \Delta t$. At point A of Fig. 7d the first order term tends to increase ρ but the second order term, which is negative, tends to decrease it. The same can be said of point C, with the signs reversed. Consequently, the density distribution tends to freeze in an oscillatory pattern.

In conclusion, the fact that a certain numerical technique has been proven to be a valid approximation of a continuous differentiable flow does not make its use legitimate across a discontinuity. All mathematical proofs founded on differentiability are invalid and the numerical consequences of doing something mathematically wrong appear as wiggles on the high pressure side of the discontinuity. An accurate steady state solution cannot be reached asymptotically since, once the wiggles are formed, the numerical evolution has very little in common with the physical evolution.

In addition, one can easily see experimentally that a steady state with discontinuities is numerically unstable, if treated with the Lax-Wendroff

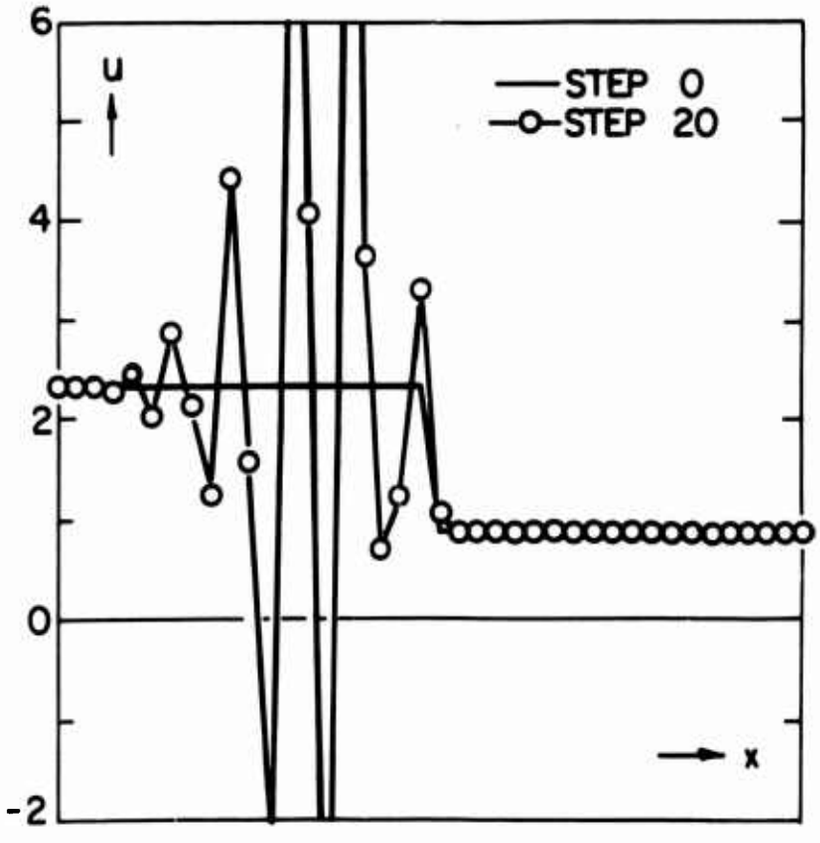

FIG. 8
VELOCITY DISTRIBUTION ACROSS A STEADY SHOCK, COMPUTED BY THE LAX-WENDROFF SCHEME WITH NO ARTIFICIAL VISCOSITY

scheme , even if the equations are in conservation form, when the discontinuities lie inside the computational region. A minor perturbation in the assigned data generates non-zero derivatives and triggers an unsteady, non-physical evolution. See Fig. 8 where u is plotted after computing 20 steps of a steady flow (corresponding to a Mach 2 shock) by the original Lax-Wendroff technique, with $\Delta t/\Delta x = .2$. The initial values were all exact except that u, at one point, had an error of the order of 10^{-4}. *

1.5 Inconveniences of artificial viscosity.

The argument developed in the preceding section is based on the assumption that there is no artificial viscosity, but it holds as long as the artificial viscosity is too small. It is clear that the shock transition cannot be confined to a single mesh interval. It is shown in Ref. 7 that the same conclusion is reached for a viscous flow. Qualitatively, our argument agrees with Crocco's analysis of a shock in a viscous flow (Ref. 11). In Crocco's paper the equations are somewhat simplified and a different numerical scheme is used.

By so doing, it is found that certain distributions of wiggles are the only possible numerical solution of the shock problem if the mesh size is too small with respect to the shock thickness. A typical condition found by Crocco is, for example,

$$\Delta x < \delta/2$$

where δ is the shock thickness defined by the ratio of the velocity jump to the maximum slope of the velocity distribution. If Lax-Wendroff's scheme

* The program used to compute this case is reported in Appendix 1. For the reader's peace of mind it should be mentioned that no instabilities appear if the initial values are all exact.

is used, the wiggle distribution about the shock is asymmetrical. The amplitude of the oscillations is much higher on the high-pressure side than on the low-pressure side.

The above considerations show that the perspectives for a practical usage of artificial viscosity are rather gloomy. Of course, artificial viscosity makes the numerical procedure once more mathematically legitimate. However, one faces the unpleasant choice between

(i) a large viscosity (to maintain a coarse mesh and a short computational time); but, then, the problem solved numerically is not the original inviscid problem.

(ii) a fine mesh (to reduce the shock thickness and the dissipative effects in general to acceptable values); but then, the price to be paid in terms of computational time becomes too high.

In the simple problem examined in the preceding sections, the damaging effects of artificial viscosity are not as strong as in more complicated problems. In fact, in most of the computational region the flow is uniform; all derivatives are zero, and the artificially viscous terms are zero. In multi-dimensional problems where non-uniform steady states can be reached, the steady state affected by artificial viscosity is generally different from the physical one for inviscid flow. For example, if Lax's technique is used, the values of all physical parameters become so distributed that their time increments exactly balance the errors due to averaging (Ref. 8).

2. The problem of the accelerating piston.

We are going now to examine a problem which is more interesting than the shock separating two uniform regions and which leads to a number of practical applications. It is the problem of what flow is produced in a gas at rest by a piston moving at variable speed. Let $x = b(t)$ be the trajectory of the piston. Let us assume that the piston was kept at rest when $t < 0$ and its motion starts at $t = 0$. Let us also assume that the initial speed of the piston, $b(0)$, is zero. For $t > 0$ we will assume that $b(t)$ is analytic and regular.

Let the pressure and density of the gas at rest be the reference values, p_{ref} and ρ_{ref}, and let a reference length, x_{ref}, be chosen arbitrarily. A reference velocity is then defined as $\sqrt{p_{ref}/\rho_{ref}}$ and a reference time as $x_{ref}/\sqrt{p_{ref}/\rho_{ref}}$. In addition, let

$$\mathcal{J} = \frac{p}{\rho}\,\frac{\rho_{ref}}{p_{ref}}, \qquad P = \ln \frac{p}{p_{ref}}, \qquad S = \gamma \ln \mathcal{J} - (\gamma - 1)\, P \tag{21}$$

In non-dimensional form, the equation of motion can be written as follows*:

$$\begin{aligned} &P_t + u\,P_x + \gamma\,u_x = 0 \\ &u_t + u\,u_x + \mathcal{J}\,P_x + 0 \\ &S_t + u\,S_x = 0 \end{aligned} \tag{22}$$

The characteristics are defined by

$$\lambda = \frac{dx}{dt} = u \pm a \tag{23}$$

where a is the local speed of sound, $a = \sqrt{\gamma}$. We will say that the characteristics belong to the first or to the second family if the upper or lower

---

* The theoretical background supporting the information contained in equations (28) to (31) is assumed as known and can be found in Ref. 9.

sign in (23) is taken, respectively. The compatibility equations along the characteristics are

$$\begin{aligned} &\text{I} && a\,dP + \gamma\,du = 0 \\ &\text{II} && a\,dP - \gamma\,du = 0 \end{aligned} \tag{24}$$

If the entropy is constant throughout, the compatibility equations can be integrated and recast in the form:

$$\begin{aligned} &\text{I} && \frac{2}{\gamma-1}\,a + u = 2r \\ &\text{II} && \frac{2}{\gamma-1}\,a - u = 2s \end{aligned} \tag{25}$$

where r and s are constant along the characteristics. The first characteristic of the I family issuing from the point ($x = 0, t = 0$) is the line

$$x = \sqrt{\gamma}\,t \tag{26}$$

This line divides the piston-driven flow from the gas at rest. As long as characteristics of the I family do not coalesce, the region above such a line is a simple, isentropically compressive wave, corresponding to a constant value of s . The value of u at a point (x,t) in the wave can be exactly computed as follows.

Let τ be the value of t at which the I-characteristic passing through the point issues from the piston (Fig. 9). Along such line, u, a and λ are constant, so that the line is straight and defined by

$$x = b(\tau) + \left[\dot{b}(\tau) + a_1(\tau)\right](t - \tau) \tag{27}$$

where $a_1(\tau)$ is the speed of sound on the piston at time τ. Since s has the same value inside the simple wave and in the gas at rest,

$$s = \frac{\sqrt{\gamma}}{\gamma - 1} \tag{28}$$

from (25.II) we obtain

$$\frac{2}{\gamma-1}\, a_1(\tau) - \dot{b}(\tau) = \frac{2\sqrt{\gamma}}{\gamma-1} \tag{29}$$

that is,

$$a_1(\tau) = \sqrt{\gamma} + \frac{\gamma-1}{2}\, \dot{b}(\tau) \tag{30}$$

By replacing this value of $a_1(\tau)$ into (27)

$$x = b(\tau) + \left[\sqrt{\gamma} + \frac{\gamma+1}{2}\, \dot{b}(\tau)\right](t - \tau) \tag{31}$$

is the equation of a I-characteristic in the simple wave.

Suppose now that one wants to know the u-distribution along the x-axis at a given time t_1. Equation (31) should be solved for τ, after replacing t by t_1. Then,

$$u(x, t_1) = \dot{b}(\tau) \tag{32}$$

The derivative of u with respect to x is

$$u_x(x, t) = \ddot{b}(\tau)\, \frac{\partial \tau}{\partial x} \tag{33}$$

where $\frac{\partial \tau}{\partial x}$ is computed from (31) at constant t:

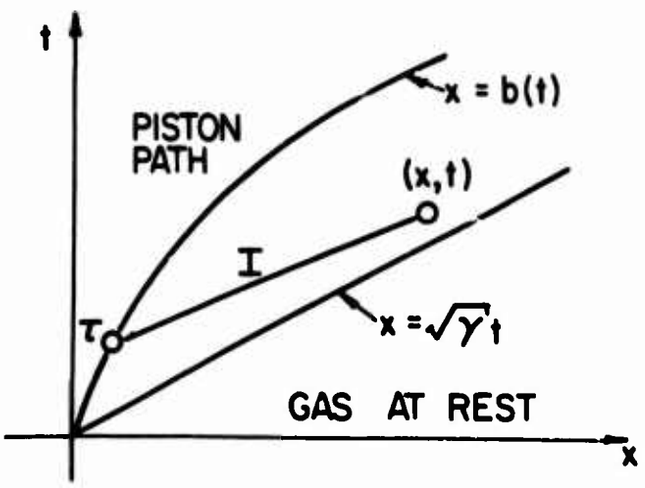

FIG. 9 FLOW PRODUCED BY AN ACCELERATING PISTON

$$\frac{\partial \tau}{\partial x} = \frac{1}{\frac{\gamma+1}{2}\ddot{b}(\tau)(t-\tau) - \sqrt{\gamma} - \frac{\gamma-1}{2}\dot{b}(\tau)} \tag{34}$$

so that

$$u_x = \frac{2\ddot{b}(\tau)}{(\gamma+1)\ddot{b}(\tau)(t-\tau) - 2\sqrt{\gamma} - (\gamma-1)\dot{b}(\tau)} \tag{35}$$

Similarly, the derivative of u with respect to t is computed:

$$u_t = - \frac{\ddot{b}(\tau)\left[2\sqrt{\gamma} + (\gamma+1)\dot{b}(\tau)\right]}{(\gamma+1)\ddot{b}(\tau)(t-\tau) - 2\sqrt{\gamma} - (\gamma-1)\dot{b}(\tau)} \tag{36}$$

As long as the denominator in (35) and (36) does not vanish, the derivatives of u are continuous and differentiable, except along the first characteristic, defined by (26), if the initial acceleration of the piston is not zero.

When the characteristics coalesce, they define an envelope, which can be found by differentiating (31) with respect to τ:

$$\frac{\gamma+1}{2}\ddot{b}(\tau)(t-\tau) - \sqrt{\gamma} - \frac{\gamma-1}{2}\dot{b}(\tau) = 0 \tag{37}$$

and eliminating τ between (31) and (37), or else, considering (31) and (37) as the parametric equations of the envelope:

$$\begin{cases} x = b(\tau) + \left[\sqrt{\gamma} + \frac{\gamma+1}{2}\dot{b}(\tau)\right]\frac{2\sqrt{\gamma} + (\gamma-1)\dot{b}(\tau)}{(\gamma+1)\ddot{b}(\tau)} \\ \\ t = \tau + \frac{2\sqrt{\gamma} + (\gamma-1)\dot{b}(\tau)}{(\gamma+1)\ddot{b}(\tau)} \end{cases} \tag{38}$$

As for the point where the characteristics coalesce, we must distinguish between two cases.

1) The initial acceleration of the piston, $\ddot{b}(0)$, is different from zero. In this case, we can prove that the curve defined by (38) is tangent to the first I-characteristic, defined by (26). Indeed, if $\tau=0$ (and, then,

$b(\tau)=0$, $\dot{b}(\tau)=0$), it is easily seen that x and t as defined by (38) satisfy (26). In addition, dx/dt, computed from (38), turns out to be equal to $\sqrt{\gamma}$. The location of the first characteristic and of the envelope is shown in Fig. 10. Point A, defined by

$$t_A = \frac{2\sqrt{\gamma}}{(\gamma+1)\ddot{b}(0)} \tag{39}$$

is their common point and is also the point where the characteristics coalesce, that is, the origin of a shock wave.

It is worth studying how the distribution of a typical parameter, say u, steepens up in the vicinity of the first characteristic as time increases, until its slope becomes imfinitely large at A. From (35) with $\tau = 0$, it follows that

$$u_x = \frac{2\ddot{b}(0)}{(\gamma+1)\ddot{b}(0)\,t - 2\sqrt{\gamma}} \tag{40}$$

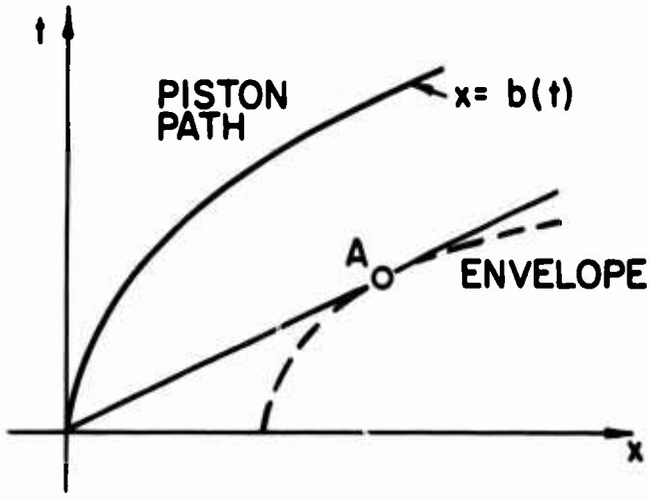

FIG. 10 ENVELOPE OF CHARACTERISTICS FOR THE CASE OF FINITE INITIAL ACCELERATION

Fig. 11 shows u_x as a function of t along the first characteristic, in the case where $\ddot{b}(0) = 2$, $\gamma = 1.4$. Note that the motion of the piston does not affect this steepening process. In fact, the right-hand side of (40) contains only the parameter $\ddot{b}(0)$. Therefore, regardless of what the phenomenon is in the rest of the simple wave, the value of u_x always becomes infinite at point A. Fig. 12* shows a number of cross-sectional plots of u(x) at different times between t = 0 and $t = t_A$ for the case where the piston path is defined by

$$b = t^2 \tag{41}$$

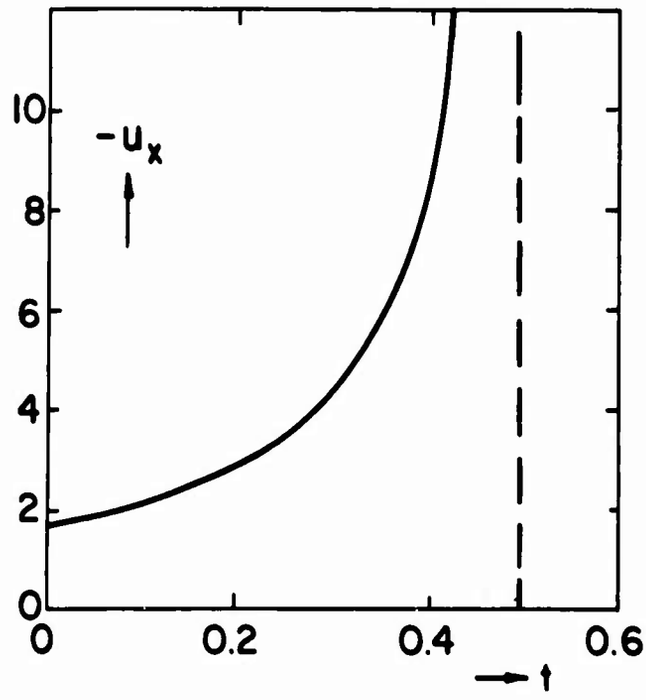

FIG. 11 PLOT OF u_x AS A FUNCTION OF TIME ALONG THE FIRST CHARACTERISTIC IN THE FLOW PRODUCED BY A PISTON MOVING WITH A FINITE INITIAL ACCELERATION

* Drawn by a Stromberg-Carlson 4020 plotter.

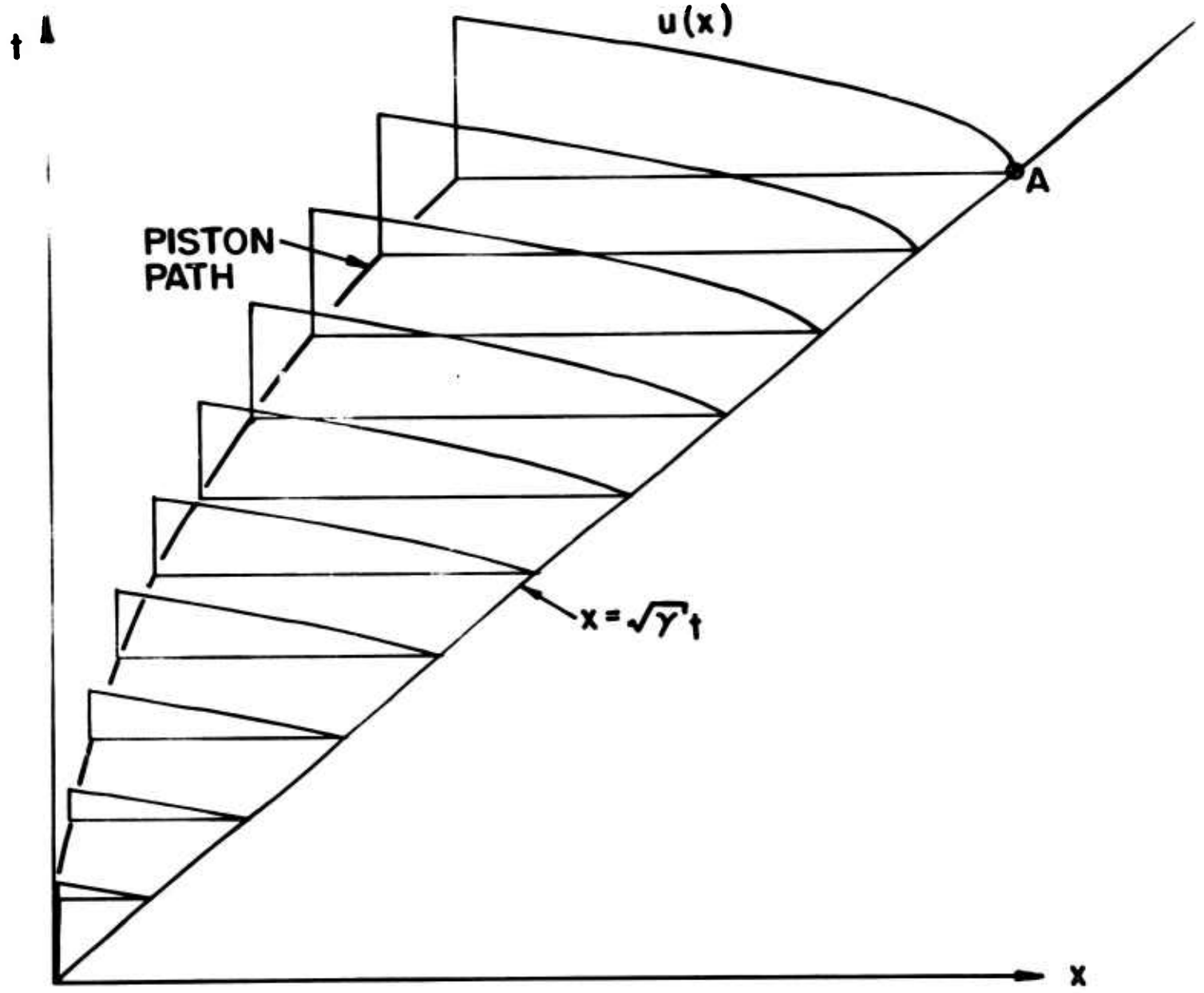

FIG. 12 EXACT PLOTS OF u(x) AT VARIOUS TIMES IN THE FLOW PRODUCED BY A PISTON MOVING WITH THE LAW $x_p = t^2$

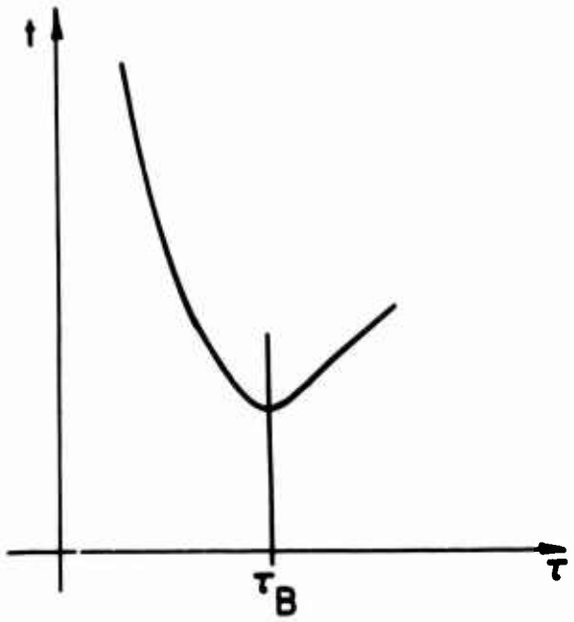

FIG. 13 PROVING THE EXISTENCE OF A CUSP IN THE ENVELOPE OF CHARACTERITICS WHEN THE PISTON HAS NO INITIAL ACCELERATION

2) The initial acceleration of the piston is zero. In this case u_x on the first I-characteristic, as given by (40),is identically zero and no steepening of the u(x) curves occurs. This result suggests that no coalescence of characteristics occurs along the first characteristic. The envelope no longer has the form shown in Fig. 10.

To find what is the shape of the envelope, consider the second of (38) which gives t on the envelope as a function of τ. At $\tau = 0$, t is infinite. For all $\tau > 0$, since $\dot{b}(\tau) > 0$, $\ddot{b}(\tau) > 0$ for an accelerating piston, t is positive. If $\ddot{b}(\tau)$ does not vanish for $\tau > 0$, then t tends to ∞ again when τ increases indefinitely. If $\ddot{b}(\tau)$ vanishes at some $\tau = \tau_1$, there t becomes infinite. In any case, $t(\tau)$ on the envelope must have a minimum (Fig. 13) at a certain value τ_B defined by

$$\left(\frac{dt}{d\tau}\right)_B = \frac{1}{\gamma+1}\left[2\gamma - \frac{2\sqrt{\gamma} + (\gamma-1)\dot{b}(\tau_B)}{\ddot{b}^2(\tau_B)}\, b(\tau_B)\right] = 0 \qquad (42)$$

Consequently, for increasing τ, t first decreases and then increases, and

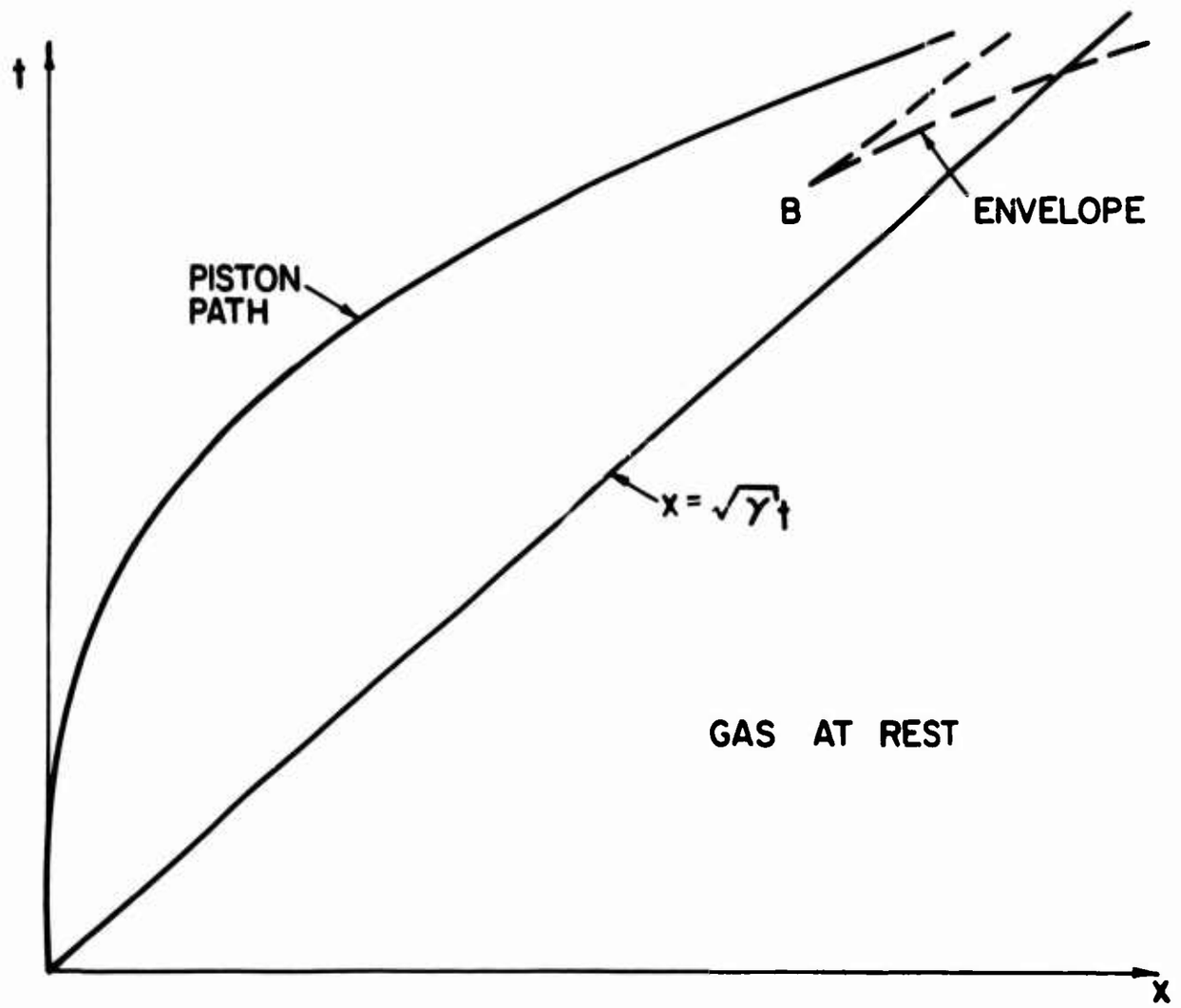

FIG. 14 ENVELOPE OF CHARACTERISTICS FOR THE FLOW PRODUCED BY A PISTON MOVING WITH THE LAW $x_p = t^3$

the envelope is shaped as in Fig. 14, with a cusp at B. The location of the cusp now depends on the nature of the piston path. Note that u_x becomes infinite at B because u_x is infinite along the entire envelope, as one can see by combining (35) and the second of (38). Therefore, the nature of the u-distribution at the origin of a shock is the same whether the shock occurs at A or at B. Fig. 15 shows a number of cross-sectional plots of u(x) at different times between t = 0 and t = t_B for the case where the piston path is defined by

$$b = t^3 \tag{43}$$

2.1. Numerical treatment of the problem. First approach.

In the initial phase (prior to the coalescence of characteristics), the flow is continuous, although the first derivatives of the flow variables may be discontinuous along the I-characteristic issuing from the origin. Consequently, we may decide to use a single computational region, extending from the piston (at the left) to an arbitrary boundary located somewhere in the region of fluid at rest, where the flow parameters are well known. For simplicity, assume a right boundary moving parallel to the piston (Fig. 16), thus defined by

$$x = c(t) = b(t) + x_o \tag{44}$$

The computational region is shown in Fig. 16; it consists of a segment of the X-axis and the obvious way to relate the physical space to the computational space is to let

$$\begin{cases} X = x - b(t) \\ T = t \end{cases} \tag{45}$$

Since for any function f,

$$f_x = f_X , \quad f_t = f_T - \dot{b} f_X \tag{46}$$

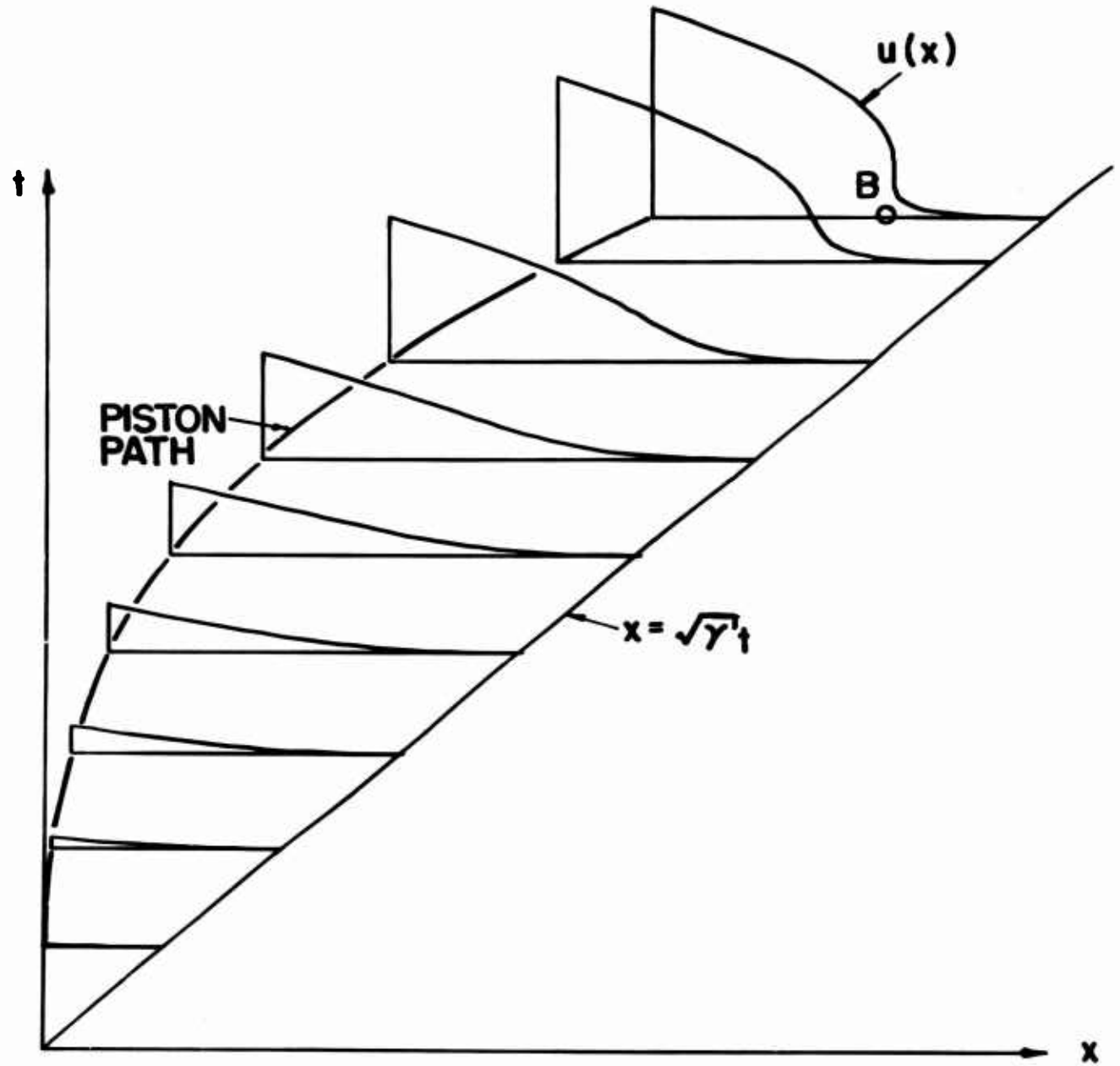

FIG. 15 EXACT PLOTS OF u(x) AT VARIOUS TIMES IN THE FLOW PRODUCED BY A PISTON MOVING WITH THE LAW $x_p = t^3$

in the computational space the equations of motion (22) are, in matrix form:

$$f_T + A f_X = 0 \tag{47}$$

with

$$f = \begin{bmatrix} P \\ u \\ S \end{bmatrix} , \quad A = \begin{bmatrix} C & \gamma & 0 \\ \gamma & C & 0 \\ 0 & 0 & C \end{bmatrix} , \quad C = u - \dot{b} \tag{48}$$

All interior points are computed as follows. Equation (47) is differentiated with respect to X and T successively:

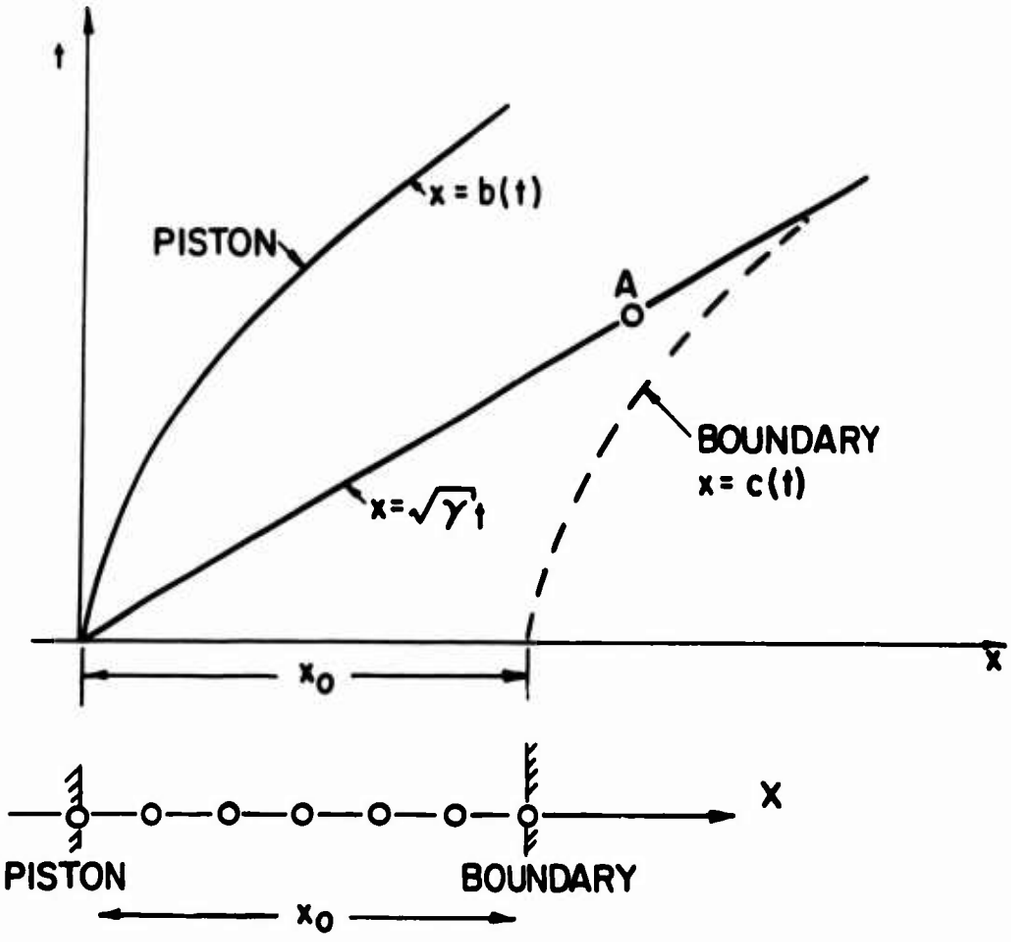

FIG. 16 FIRST DEFINITION OF A COMPUTATIONAL REGION FOR THE PROBLEM OF THE ACCELERATING PISTON

$$f_{TX} + A_X f_X + A f_{XX} = 0 \tag{49}$$

$$f_{TT} + A_T f_X + A f_{TX} = 0 \tag{50}$$

The first and second space derivatives appearing in (47), (49) and (50) are approximated by centered differences,

$$f_X \approx \frac{f^k_{n+1} - f^k_{n-1}}{2\,\Delta X} \tag{51}$$

$$f_{XX} \approx \frac{f^k_{n+1} + f^k_{n-1} - 2f^k_n}{\Delta X^2} \tag{52}$$

To evaluate A_X and A_T, note that

$$\mathcal{J} = \exp\left(\frac{\gamma-1}{\gamma} P + \frac{S}{\gamma}\right) \tag{53}$$

consequently,

$$C_X = u_X\,, \quad \mathcal{J}_X = \mathcal{J}\left(\frac{\gamma-1}{\gamma} P_X + \frac{1}{\gamma} S_X\right), \quad A_X = \begin{bmatrix} C_X & 0 & 0 \\ \mathcal{J}_X & C_X & 0 \\ 0 & 0 & C_X \end{bmatrix} \tag{54}$$

These values are used to evaluate f_{TX}. Similarly,

$$C_T = u_T - \ddot{b}\,, \quad \mathcal{J}_T = \mathcal{J}\left(\frac{\gamma-1}{\gamma} P_T + \frac{1}{\gamma} S_T\right), \quad A_T = \begin{bmatrix} C_T & 0 & 0 \\ \mathcal{J}_T & C_T & 0 \\ 0 & 0 & C_T \end{bmatrix} \tag{55}$$

and, since u_T, P_T and S_T are furnished by (47), we have all the necessary elements to compute f_{TT}. Then (16) is used to proceed one step ahead in time. As a matter of fact, the entropy is identically zero in this problem (which we consider finished once the characteristics coalesce), the third equation could be dropped and the terms S, S_X, S_T eliminated; but we pre-

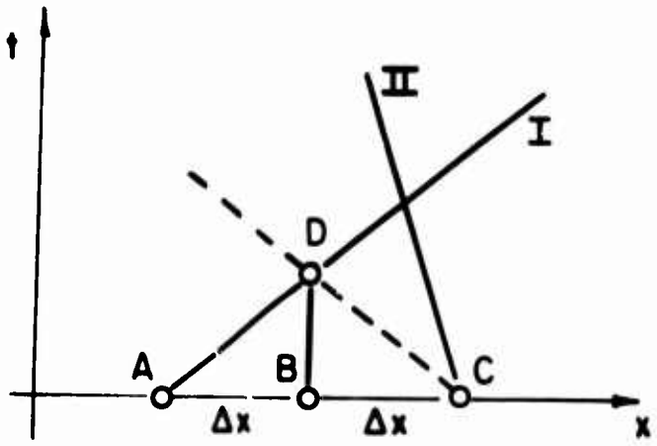

FIG. 17 TO DETERMINE THE RATIO BETWEEN Δt AND Δx

fer to keep them to show a general pattern to be followed for non-isentropic flows.

The boundary values in the present case are extremely easy to compute. At the piston, $u = b$, $S = 0$, a is given by (30) with t instead of τ, and P follows from (21). At the free boundary on the right, $u = 0$, $S = 0$, $P = 0$.

The stepsize in time, ΔT, is determined as follows. Of the two characteristics, consider the one which has the larger slope with respect to the t-axis (for example the one labeled I in Fig. 17); such a slope is safely defined by $|u| + a$. If A, B and C are the three points used in the computation, draw a line issuing from C and symmetric to I. Let D be the intersection of I and its symmetric. Every value of Δt less than BD satisfies the Courant-Friedrichs-Lewy rule (Ref. 10). Now, $BD = \Delta x/(|u| + a)$ and so we assume

$$\Delta t = .7 \frac{\Delta x}{|u| + a} \tag{56}$$

The coding of this program is very easy; a sample code is shown in Appendix 2 and it should be self-explanatory. The "output" routine is not reported here and is left to the reader to be shaped according to his

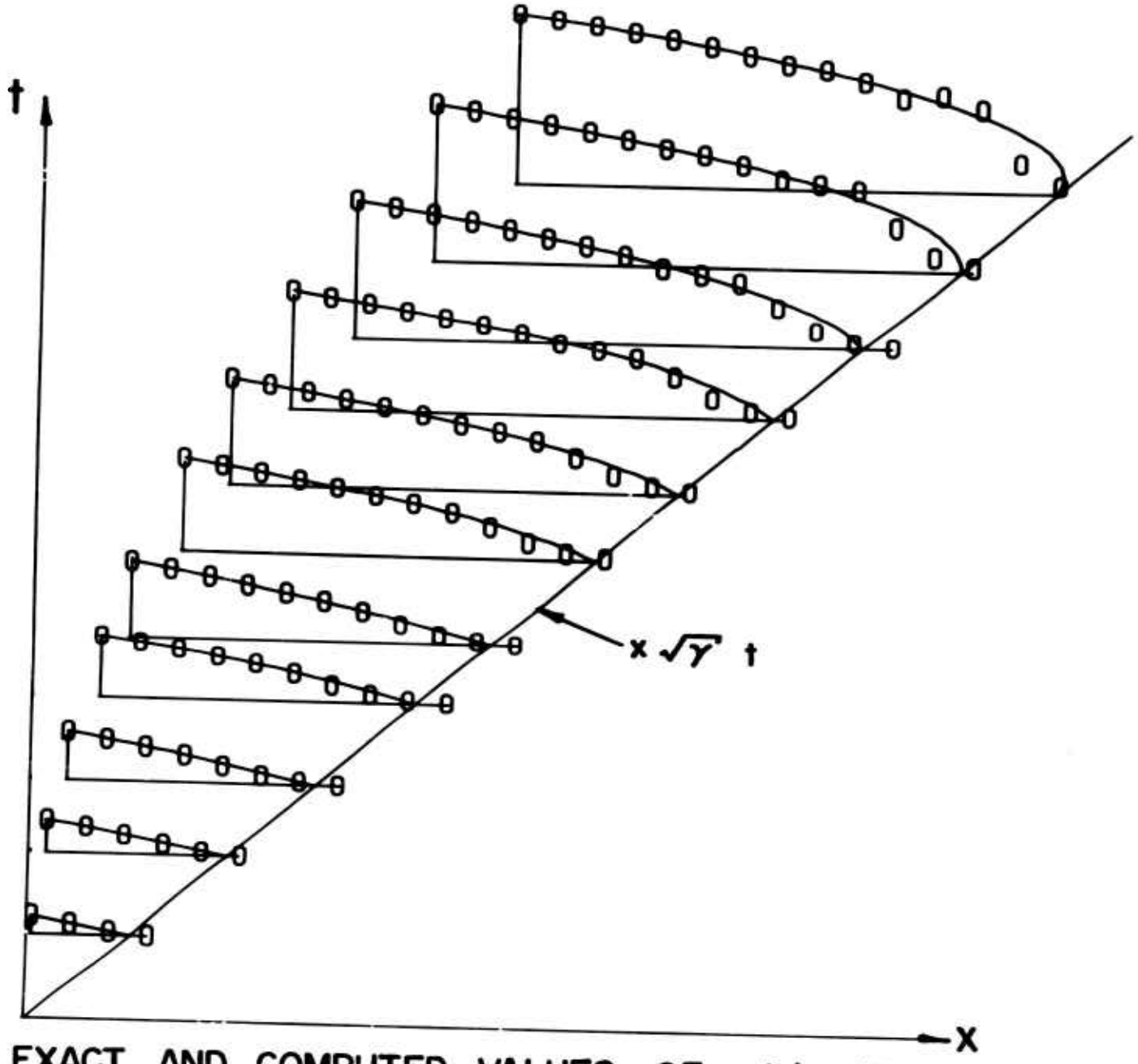

FIG. 18 EXACT AND COMPUTED VALUES OF u(x) AT VARIOUS TIMES IN THE FLOW PRODUCED BY A PISTON MOVING WITH THE LAW $x_p = t^2$

preferences. The "piston" routine is not shown either; it must provide the necessary data to define the piston path, b(t) and its derivatives $\dot{b}$ and $\ddot{b}$.

2.2 The case of discontinuous initial acceleration.

We apply now the program to the two problems mentioned in Section 2. First, we assume the piston path as defined by (41). We know that u_x is discontinuous along the $x = \sqrt{\gamma}\, t$ line and that it becomes infinite at

$$t_A = \frac{\sqrt{\gamma}}{\gamma+1} = .4929 \qquad (\text{for } \gamma = 1.4) \tag{57}$$

where a shock should originate. We are interested in seeing what kind of difficulties and inaccuracies arise because of the discontinuities in the first derivatives. Such discontinuities are not as strong as the ones across a shock but still they make the flow parameters not twice differentiable along the first I-characteristic. So, we expect a progressive worsening of the computed flow in that neighborhood, until a pattern similar to the one described in Fig. 7 builds up as representative of the shock.

Fig. 18 shows some of the results (values of u)*. The computed values are shown as circles, whereas the exact distribution is represented by a continuous line. Point A, as defined by (39), is also shown. We see that, long before the characteristics coalesce, the computed values deteriorate in the vicinity of the line where the derivatives of u are discontinuous. In addition, once the characteristics coalesce into a shock, a wiggle starts building up. According to our analysis (Fig. 7), we should fit a shock two

---

* The mesh has nodes spaced .025 apart. There are no other nodes, in the range of interest, except those shown in Fig. 3.18. However, not all the steps are shown. The computation, with a total of 50 intervals across, takes about 6 seconds on a CDC 6600 computer (including compilation). The computation has been repeated on an IBM 360/50 computer, coupled with the Stromberg-Carlson 4020 plotter, to obtain the figure.

nodal points at the right of the wiggle. We will see later on how to treat the shock as a discontinuity; by doing so (here we mention the result without presenting any figure), the shock would quickly adjust itself to the right position, and the values on the high-pressure side would improve rapidly. However, the results are far from perfect in the time space starting at about $t = .4$ and lasting for a time of the order of 1. This effect is due not to the formation of the shock but to the discontinuity in the derivatives of the velocity. We will return on the subject on Section 3.3.

2.5 The case of continuous initial acceleration.

Now the same program is applied to the case where the piston path is defined by (43). The derivatives of the velocity are continuous everywhere and the coalescence of characteristics occurs at point B, defined by (43). With $\gamma = 1.4$, we find $\tau_B = .389$ and, from (38),

$$t_B = .844, \quad x_B = .8415 \tag{58}$$

Since in this case we are not forcing the numerical computation to approximate derivatives where they do not exist, we anticipate a much better behavior of the computed results prior to point B. The expectation is confirmed by Fig. 19. Again, as in Fig. 18, the exact distribution of $u(x)$ is represented by a continuous line, and the computed values (at mesh points spaced .2 apart) by circles. The circles fall exactly on the lines, as long as $t < t_B$. In addition, it can be noted that the numerical technique is capable of handling a very sharp transition with no trouble.

If the computation is continued beyond $t = t_B$, however, the effects of neglecting a shock begin showing up and a wiggle if formed where anticipated (two mesh points at the left of the approximate location of the shock).

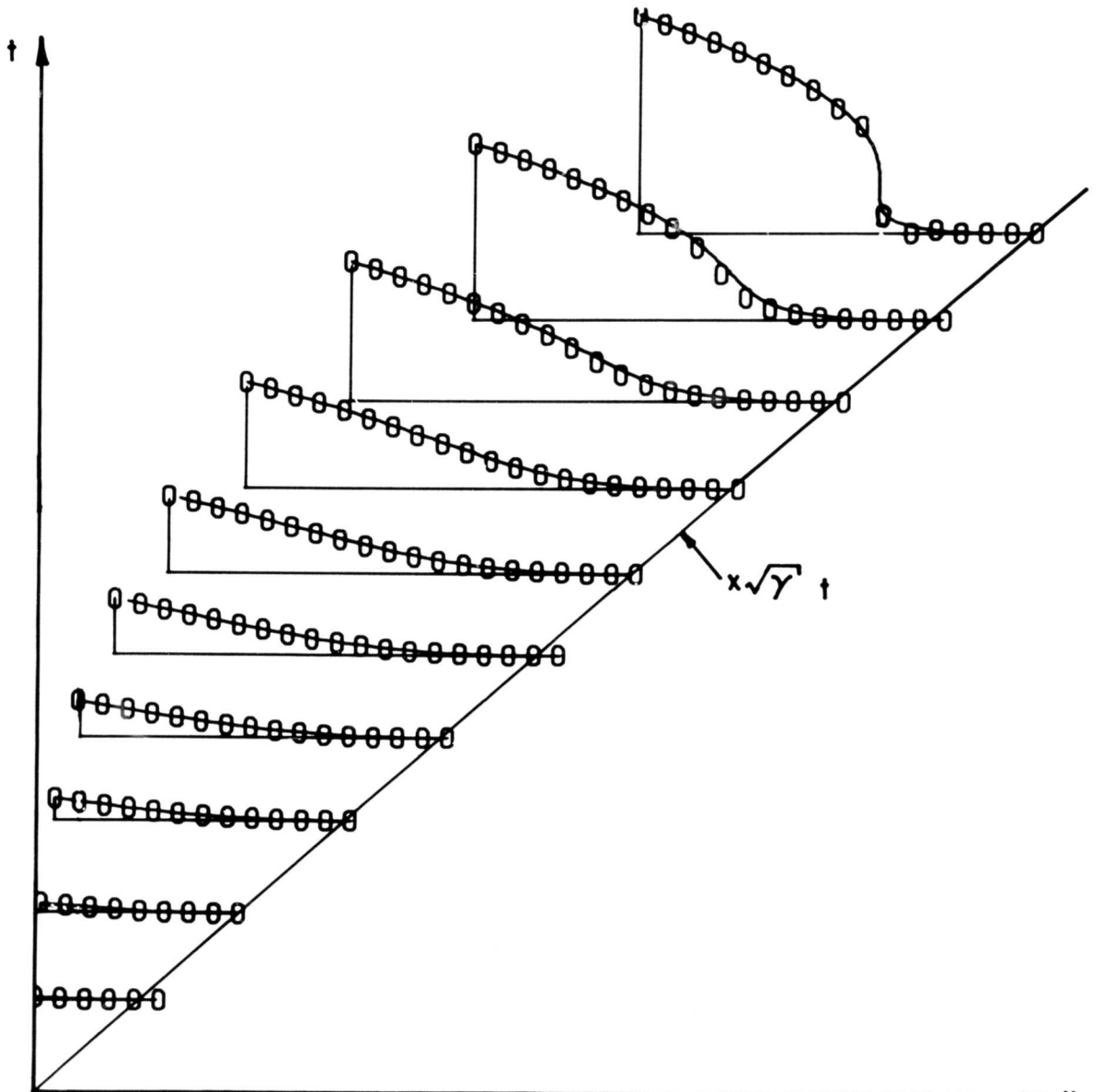

FIG. 19 EXACT AND COMPUTED VALUES OF u(x) AT VARIOUS TIMES IN THE FLOW PRODUCED BY A PISTON MOVING WITH THE LAW $x_p = t^3$

2.4. An expansion problem with discontinuous initial acceleration.

So far, we have found experimental confirmation to the points made above. Discontinuities in the flow parameters, such as shocks, originate wiggles. Discontinuities in their derivatives are not equally catastrophic but deteriorate the numerical results in a wider and wider region surrounding the location of the discontinuity. In both cases, the discontinuities should be treated as boundary points.

Before analyzing how this can be done, it is interesting to see how the discontinuity in the derivatives of the flow variables affects an expanding flow. To this effect, we study the expanding counterpart of the case presented in Section 2.2. Let the piston now move to the left, and its path be defined by

$$x = - t^2 \tag{59}$$

Again, (35) and (36) show that u_x and u_t are discontinuous on the first I-characteristic. For example,

$$u_x = \frac{2}{(\gamma-1)t + \sqrt{\gamma}} \tag{60}$$

However, u_x decreases with increasing t, and we may anticipate that the effects of the discontinuity in u_x will become less and less relevant with increasing time; and since they are not strong to begin with, they should be irrelevant throughout.

The anticipation is confirmed by Fig. 20, drawn with the same criteria as Figs. 18 and 19. The computed values (circles) lie very close to the theoretical line. To see the effects of neglecting the discontinuity one has to enlarge the u-scale by one order of magnitude.

3. Treatment of a shock on a boundary.

In this section we examine in detail a technique which combines the interior point computation described above with a treatment of one boundary

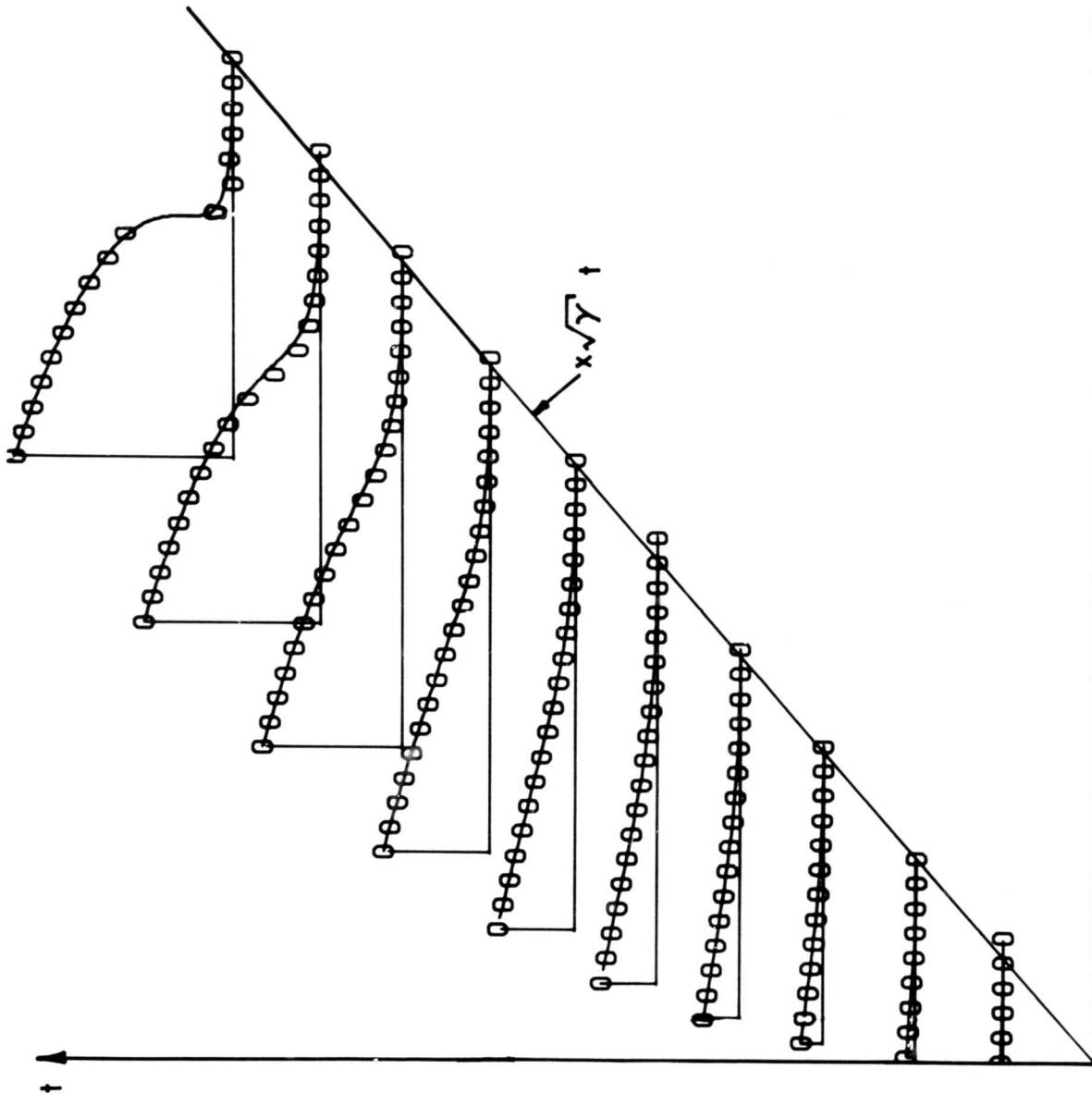

FIG. 19 EXACT AND COMPUTED VALUES OF u(x) AT VARIOUS TIMES IN THE FLOW PRODUCED BY A PISTON MOVING WITH THE LAW $x_p = t^3$

2.4. An expansion problem with discontinuous initial acceleration.

So far, we have found experimental confirmation to the points made above. Discontinuities in the flow parameters, such as shocks, originate wiggles. Discontinuities in their derivatives are not equally catastrophic but deteriorate the numerical results in a wider and wider region surrounding the location of the discontinuity. In both cases, the discontinuities should be treated as boundary points.

Before analyzing how this can be done, it is interesting to see how the discontinuity in the derivatives of the flow variables affects an expanding flow. To this effect, we study the expanding counterpart of the case presented in Section 2.2. Let the piston now move to the left, and its path be defined by

$$x = - t^2 \tag{59}$$

Again, (35) and (36) show that u_x and u_t are discontinuous on the first I-characteristic. For example,

$$u_x = \frac{2}{(\gamma-1)t + \sqrt{\gamma}} \tag{60}$$

However, u_x decreases with increasing t, and we may anticipate that the effects of the discontinuity in u_x will become less and less relevant with increasing time; and since they are not strong to begin with, they should be irrelevant throughout.

The anticipation is confirmed by Fig. 20, drawn with the same criteria as Figs. 18 and 19. The computed values (circles) lie very close to the theoretical line. To see the effects of neglecting the discontinuity one has to enlarge the u-scale by one order of magnitude.

3. Treatment of a shock on a boundary.

In this section we examine in detail a technique which combines the interior point computation described above with a treatment of one boundary

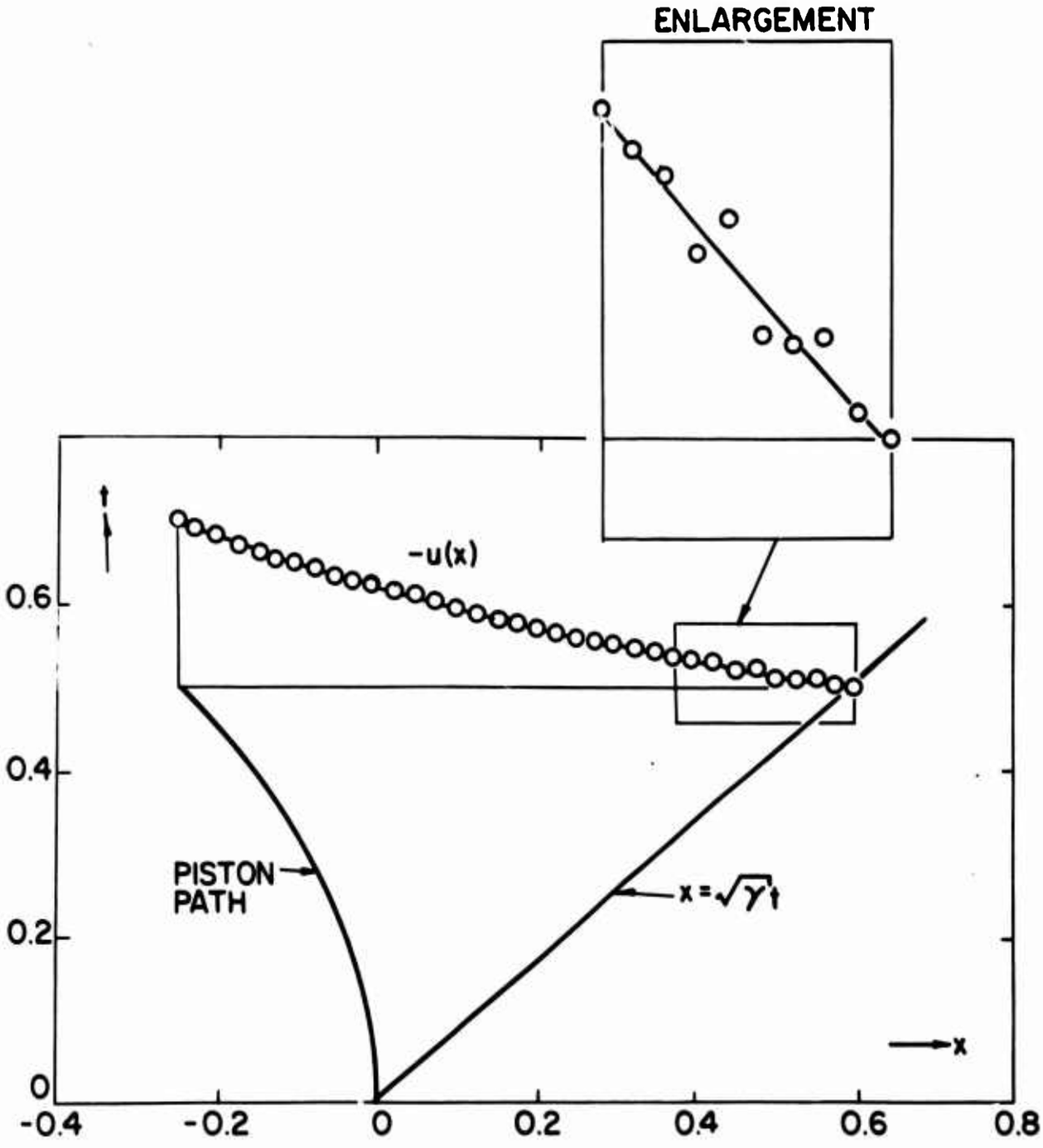

FIG. 20 COMPARISON BETWEEN EXACT VALUES AND VALUES COMPUTED AS EXPLAINED IN SECTION 2.1. PISTON PATH DEFINED BY $x_p = t^2$

as a shock. We assume that the location of the shock at a given time is known. The shock is moving at a certain speed, $W = \dot{c}(t)$, which is one of the unknowns of the problem. Consequently, the interior point computation must also be modified slightly, and we begin with it.

3.1. Computation of interior points.

Referring to Fig. 16, the following change of coordinates is necessary:

$$X = \frac{x - b(t)}{c(t) - b(t)} \qquad T = t \tag{61}$$

Since, for any function f,

$$f_x = \frac{1}{c-b} f_X \ , \quad f_t = f_T + \frac{(X-1)\dot{b} - X\dot{c}}{c - b} f_X \tag{62}$$

the equations of motion in the computational space are, in matrix form,

$$f_T + A f_X = 0 \tag{63}$$

with

$$f = \begin{bmatrix} P \\ u \\ S \end{bmatrix} , \quad A = \begin{bmatrix} C & F & 0 \\ E & C & 0 \\ 0 & 0 & C \end{bmatrix} \tag{64}$$

$$D = \frac{1}{c-b} \ , \quad C = D\left[u + (X-1)\dot{b} - X\dot{c}\right] , \quad E = D\mathcal{J} \ , \quad F = D\gamma$$

Consequently, (65)

$$D_X = 0, \ C_X = D(u_X + \dot{b} - \dot{c}), \ E_X = D\mathcal{J}_X, \ F_X = 0, \ A_X = \begin{bmatrix} C_X & 0 & 0 \\ E_X & C_X & 0 \\ 0 & 0 & C_X \end{bmatrix}$$

and (66)

$$D_T = -D^2(\dot{c}), \ C_T = D_T C / D + D\left[u_T + (X-1)\ddot{b} - X\ddot{c}\right], \ E_T = D_T\mathcal{J} + D\mathcal{J}_T, \ F_T = D_T\gamma,$$

$$A_T = \begin{bmatrix} C_T & F_T & 0 \\ E_T & C_T & 0 \\ 0 & 0 & C_T \end{bmatrix}$$

The code then proceeds as shown in Section 2.1.

3.2. Shock computation.

To compute the right boundary, where the shock is, we proceed as follows. Since the flow in front of the shock is known, only four quantities must be evaluated at the shock point, viz. P, S (or p and ρ), u, and W. The Rankine-Hugoniot conditions can be used here in the form:

$$M_1 = W/\sqrt{\gamma} \tag{67}$$

$$\gamma = \frac{2}{\gamma+1}\left(1 + \frac{\gamma-1}{2} M_1^2\right) \tag{68}$$

$$p = \frac{(\gamma+1)\rho - (\gamma-1)}{(\gamma+1) - (\gamma-1)\rho} \tag{69}$$

$$v = - W/\rho \tag{70}$$

$$u = v + W \tag{71}$$

where ρ, p, v and u are values on the high-pressure side of the shock, that is, at the point we wish to compute. Here we have five equations with six unknowns (W, M_1, ρ, p, v. u). The missing equation is the compatibility equation on the I-characteristic reaching the shock point from a point A located in the interior of the region being computed. In the physical plane

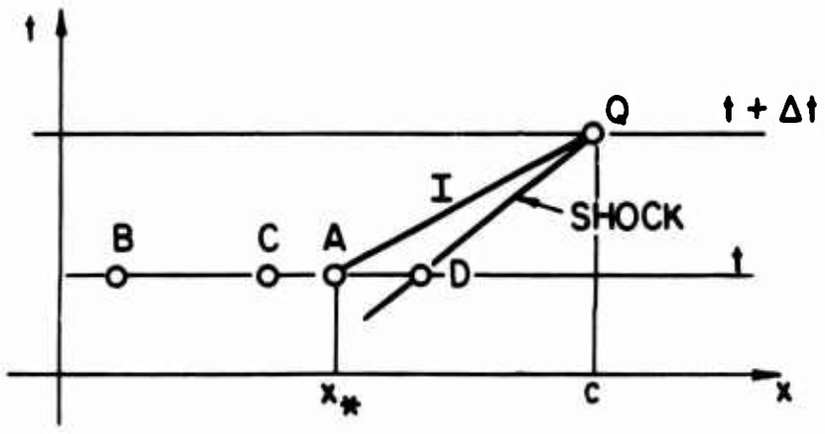

FIG. 21 COMPUTATION OF A SHOCK POINT

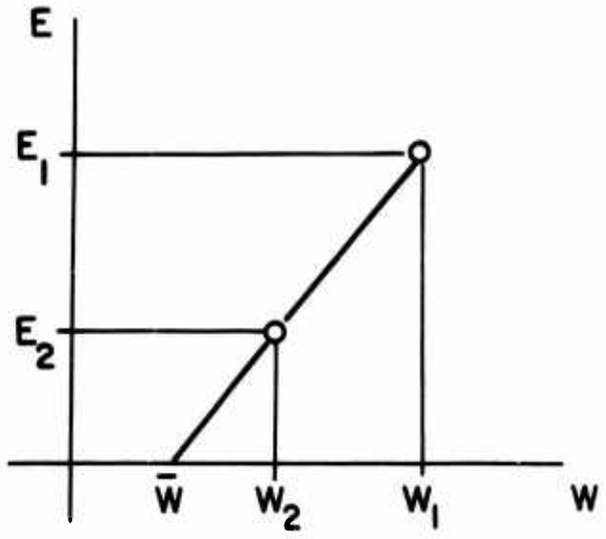

FIG. 22 NEWTON'S RULE TO MINIMIZE ERRORS

the situation appears as in Fig. 21. All values at nodal points B, C, D, ... are known at time t. The location of point A must be found and the values of the physical parameters at A (all denoted by * in what follows) must be interpolated.

To determine x_* we use the equation

$$x_* = c - (u + a)\,\Delta t \tag{72}$$

where u and a may be taken as the arithmetic averages between their values at Q and at A. The compatibility equation (24-I) can be written in the form:

$$u = u_* - \frac{a}{\gamma}(P - P_*) \tag{73}$$

where, again, a is an average value.

Equations (72) and (73), together with an interpolation scheme to determine u_*, P_*, a_*, must be added to the Rankine-Hugoniot equations above and the whole system can be solved by iteration. We describe

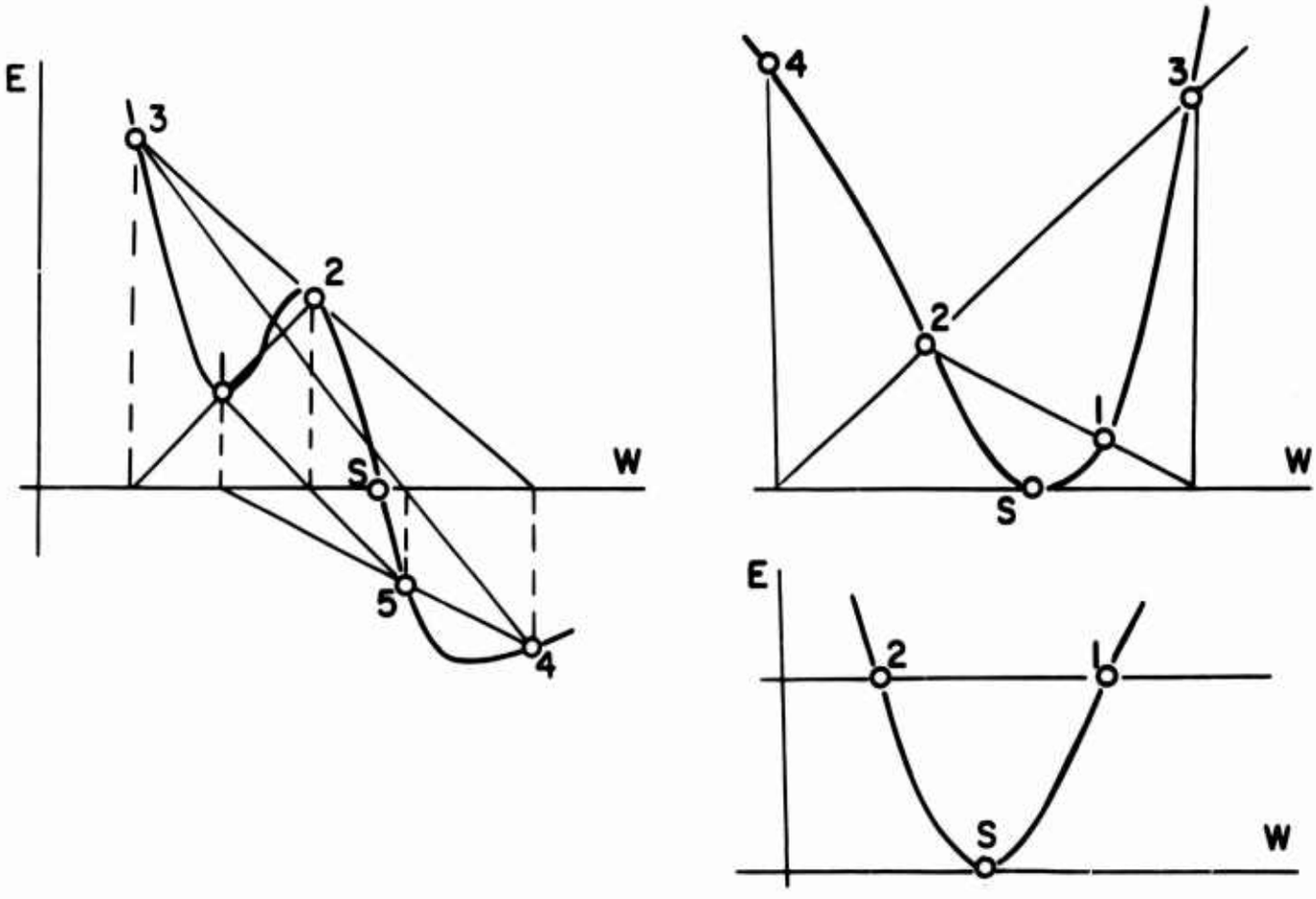

FIG. 23 EXAMPLES OF POSSIBLE FAILURES OF NEWTON'S RULE

Newton's method which generally works in a variety of problems. Two guesses of W are made, W_1 and W_2. Each time, equations (67) through (73) are used. The value of u obtained from (73) generally is different from the value obtained from (71). Call E their difference (W_1 when W_1 is used, E_2 when W_2 is used). An extrapolated value of W, $\overline{W}$, which should give a smaller value of the error E, is obtained, according to Fig. 22, as

$$\overline{W} = W_1 - E_1 \frac{W_2 - W_1}{E_2 - E_1} \tag{74}$$

Then the procedure is applied again, using W_2 instead of W_1, $\overline{W}$ instead of W_2 and E_2 instead of E_1, and reiterated until E_2 becomes less than

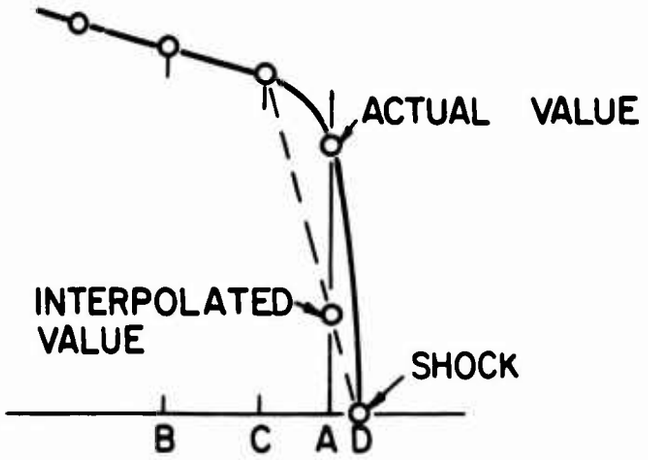

FIG. 24 INTERPOLATION BEHIND A SHOCK

a prescribed tolerance. Such a technique is not completely safe. For example, there are possibilities of being caught in a loop or of generating a divergent iteration or of dividing by zero even when a solution exists. Figure 23 shows examples of these possibilities (the exact dependence of E on W being shown by the solid line and the solution being obviously given by point S). However, such cases are highly improbable because they require the conditions shown in the figure to be satisfied to an order of accuracy equal to the number of significant figures carried by the computer. Therefore, it does not pay to take special provisions for them, which would make the code cumbersome and increase the computational time.

More interesting because of its physical implications, and sometimes difficult, is the problems of interpolating values at A (Fig. 21). In most cases a linear interpolation between points C and D is sufficient. This amounts to approximate the value of any function f at A by

$$f_* = f(C) + \epsilon \left[f(D) - f(C) \right] \tag{75}$$

where

$$\epsilon = \frac{x_* - x(C)}{\Delta x} \tag{76}$$

There are cases, however, where in the high pressure side of the shock the physical values are distributed as shown in Fig. 24. This is the case at the very beginning of the shock, in both problems studied above. If point A is very close to D (and this happens at the beginning of the shock, when W is practically equal to u+a) the linearly interpolated values at A are too different from the actual values. The effect of the pressure surge behind the shock is not picked up properly by the computation and the shock is not properly fed. Consequently, the strength of the shock does not grow sufficiently, the values at the shock do not grow sufficiently and, in few steps, a wiggle starts building up behind the shock. The effect is not permanent since the right values are transmitted to the region near the shock from the piston and the flow has a tendency to correct itself. See, for example, in Fig. 25, the u-distribution in the problem of Section 2.2 at successive times after the shock formed, if the technique described above and a linear interpolation at point A are used.

A much better numerical description of the physical nature of the flow in the vicinity of the shock is obtained if the values at A are considered as the average of the values extrapolated linearly from points B and C and the values interpolated linearly between points C and D*. This means that the value of any function f at A is assumed to be

$$f_* = f(C) + \left[f(D) - f(B) \right]/2 \qquad (77)$$

The results, in the same problem shown in Fig. 25, are now those of Fig. 26. The shock, as one can see, picks up strength from the very

---

* This is indeed a very easy way to improve the interpolation. One could think of other ways of doing it, for example, by interpolating on second order fits of x(u), x(P) and x(S) but such interpolations would require a great deal of additional computations which seems to be unjustified, in the light of the results obtained by using (77).

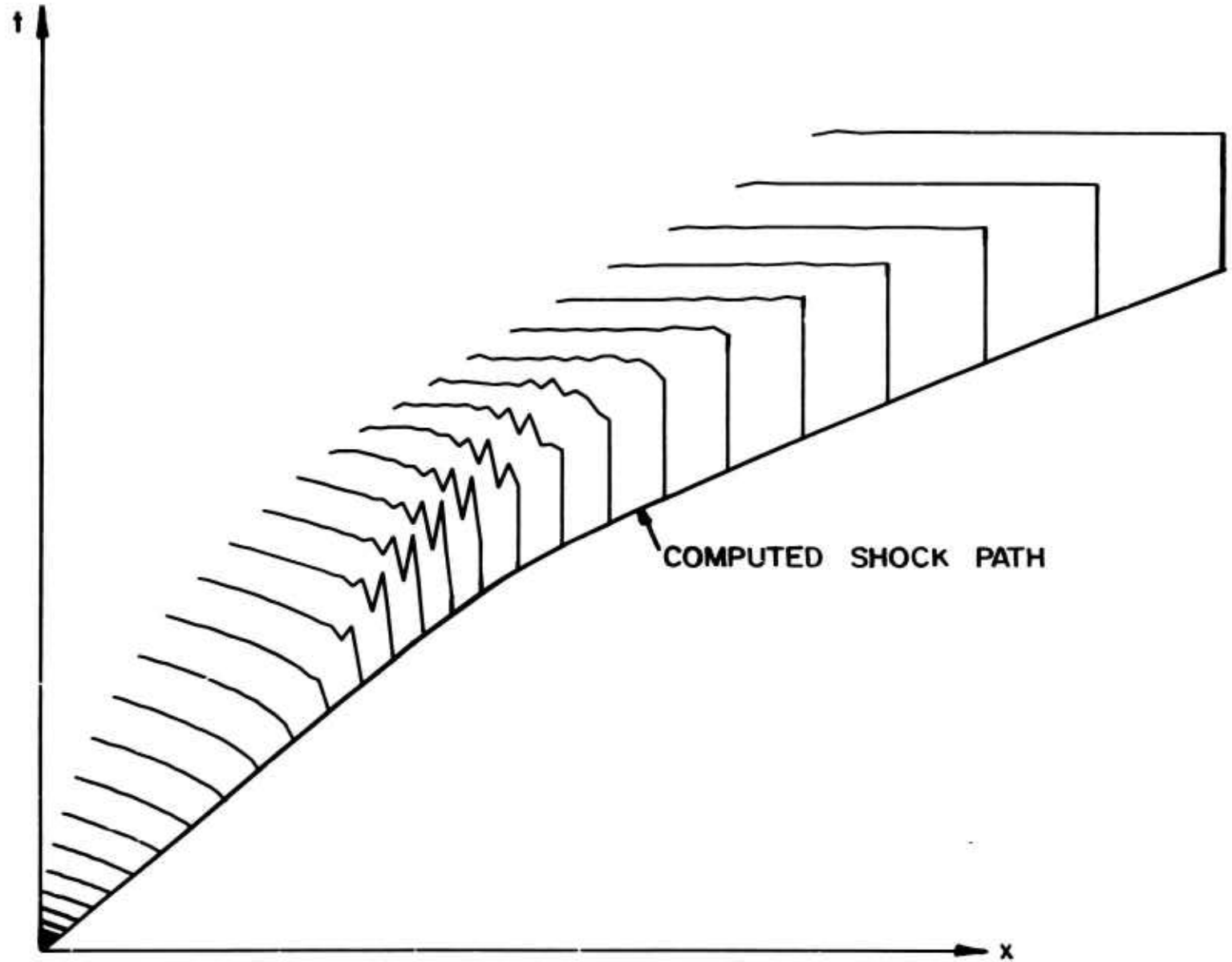

FIG. 25 COMPUTED DISTRIBUTIONS OF u(x) AT VARIOUS TIMES IN THE FLOW PRODUCED BY A PISTON ACCELERATED BY THE LAW $x_p = t^2$ UNTIL A CONSTANT SPEED IS REACHED (FIRST)

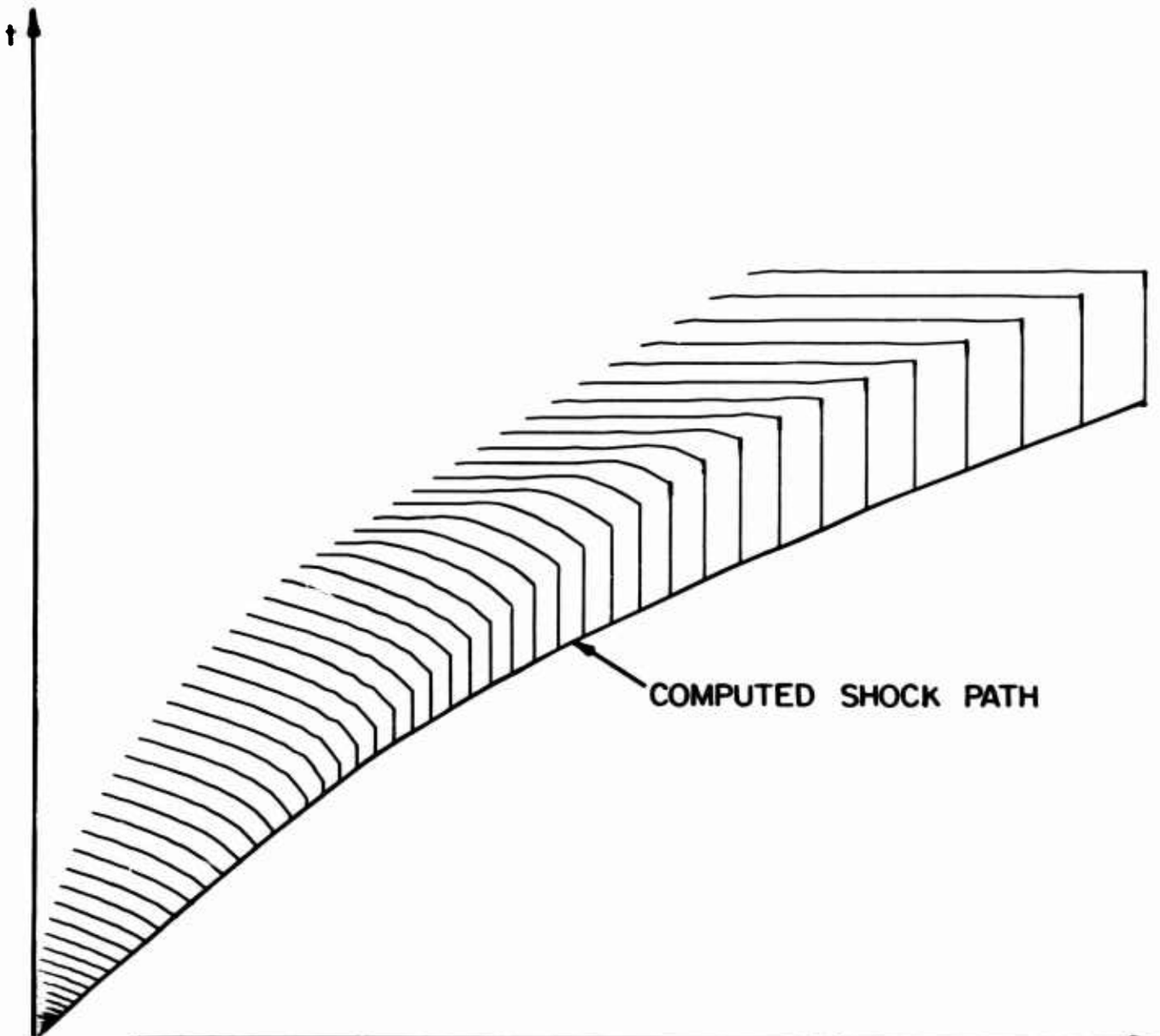

FIG. 26 COMPUTED DISTRIBUTIONS OF u(x) AT VARIOUS TIMES IN THE FLOW PRODUCED BY A PISTON ACCELERATED BY THE LAW $x_p = t^2$ UNTIL A CONSTANT SPEED IS REACHED (SECOND)

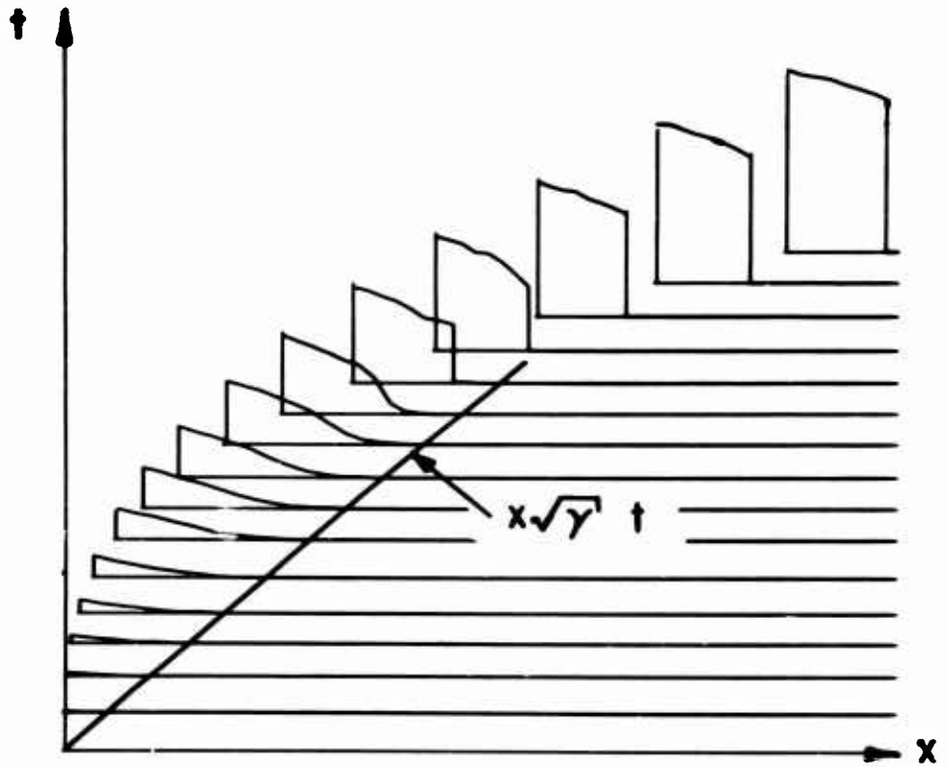

FIG. 32 COMPUTED DISTRIBUTIONS OF u(x) AT VARIOUS TIMES FOR THE FLOW PRODUCED BY A PISTON MOVING WITH THE LAW $x_p = t^3$

beginning and no wiggles appear.*

Obviously, if the distribution of values in the vicinity of the shock is not as critical as in Fig. 24, (77) is numerically equivalent to (75).

Once the values at the shock are determined, including W, the shock location at $t + \Delta t$ is obtained by simply writing that

$$c(t + \Delta t) = c(t) + W(t)\,\Delta t \qquad (78)$$

3.3 The infinitely weak shock.

Being able to compute a shock point on the boundary, we have the case of the accelerating piston with a finite initial acceleration under control. The proper way of computing it consists of assuming that a shock exists from the beginning, issuing from the origin of the (x,t) plane with a speed equal to $\sqrt{\gamma}$. In so doing, the discontinuity in u_x does not affect the computation since it takes place at a boundary point, which is assumed to be a locus of discontinuities and is treated as such. On the other hand, an infinitely weak shock is a characteristic and, since the assumed shock does not exist before $t = t_A$, during this time the boundary is the first I-characteristic itself. Point A (Fig. 10) is then reached as a boundary point and the computation can be continued beyond it indefinitely since all the computational apparatus to take care of a growing shock is available. The results (Fig. 26) are remarkably accurate and the transition from the simple wave to the shocked, non-isentropic flow is extremely smooth.

---

* In Fig. 25 and 26 the piston path is defined by

$$b = \begin{cases} t^2 & (0 \le t \le .7395) \\ 1.479t - .5469 & (t \ge .7395) \end{cases}$$

By doing so, a steady state should be reached asymptotically, where the shock Mach number is 2 and the flow is uniform between the piston and the shock. It can be seen from both figures that such a steady state is reached very rapidly. The computed shock Mach number at the time corresponding to the last plot is 2.01.

One word is in order about how to start the computation. Since the physical region to be computed vanishes at the origin, we are forced to start at some very small but finite, positive time. In general, when a similar situation occurs in a more complicated problem, one may assume that the initial distribution of physical parameters corresponds to a simple wave.

Appendix 3 contains the code for the computation from which Fig. 26 was obtained. The subroutines "piston" and "output" are omitted. By comparing Appendix 3 with Appendix 2 one can see that the subroutine which computes the interior points is not made more difficult by the stretching of the physical space into a computational space.

A further proof of the possibility of considering a characteristic as an infinitely weak shock is found if the code of Appendix 3 is applied to the expansion problem of Section 2.4. The results are omitted here. Starting with 16 mesh intervals, values correct to within 5 significant figures at least are obtained as long as the mesh size does not become gigantic.

3.4 Treatment of an imbedded shock.

In the problem of an accelerating piston with zero initial acceleration the shock is imbedded in the flow field. In this section we describe briefly how this situation is handled.

Since the inception of the shock, that is, since $t = t_B$, the flow field is split into two regions, bounded by the shock. There are, thus, two points representing the shock, one being the right boundary of the high pressure region and the other being the left boundary of the low pressure region (Fig. 27). The computation of the former is the same as outlined in Section 3.2, once the low pressure point has been evaluated. The latter is reached

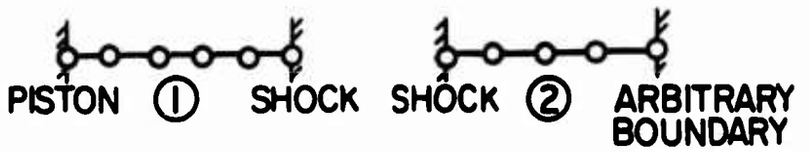

FIG. 27 TWO COMPUTATIONAL REGIONS SEPARATED BY A SHOCK

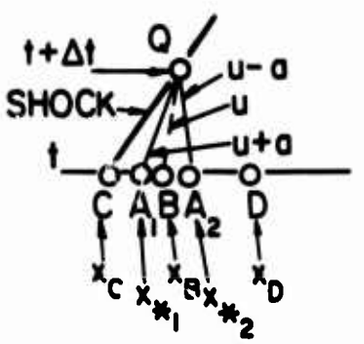

FIG. 28 COMPUTATION OF THE LOW-PRESSURE SIDE OF A SHOCK

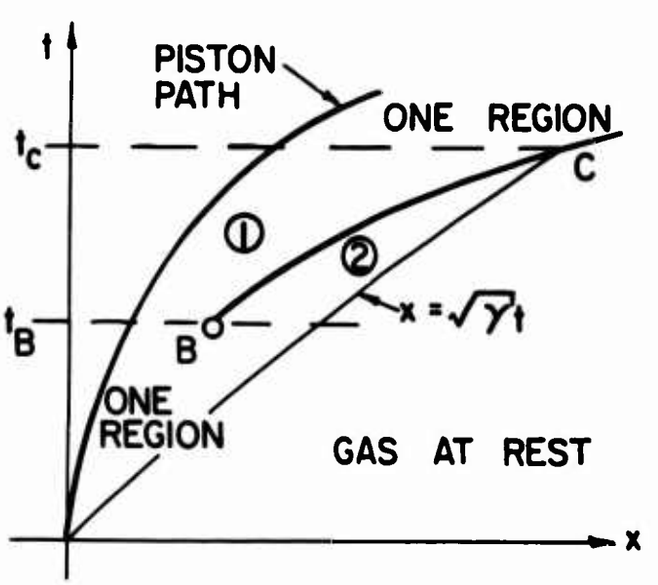

FIG. 29 COMPUTATIONAL REGIONS

by two characteristics and a particle path; therefore, two compatibility conditions and the condition of conservation of entropy can be written to determine the flow parameters (Fig. 28). In the physical plane, the locations of points A_1, A_2 and B are given by

$$\begin{cases} x_{*1} = x_Q - (u+a)\,\Delta t \\ x_{*2} = x_Q - (u-a)\,\Delta t \\ x_B = x_Q - u\,\Delta t \end{cases} \tag{79}$$

After the pertinent interpolations (in the spirit of (77)) have been made, equations (24) are applied, in the approximate form:

$$\begin{cases} P = \dfrac{a_{*1} P_{*1} + a_{*2} P_{*2} + \gamma(u_{*2} - u_{*1})}{a_{*1} + a_{*2}} \\ u = u_{*1} - \dfrac{a_{*1}}{\gamma}(P - P_{*1}) \\ S = S_B \end{cases} \tag{80}$$

The interior points in each region are treated as explained in Section 3.1, with obvious modifications (for example, what is c(t) for region 1 is b(t) for region 2).

The right arbitrary boundary of region 2 can be chosen to be the $x = \sqrt{\gamma}\,t$ line, as in the problem with finite initial acceleration. Values along that line can be safely forced to be $u = 0$, $P = 0$, $S = 0$. The line itself is prescribed, so that in region 2, $c = \sqrt{\gamma}\,t$, $\dot{c} = \sqrt{\gamma}$, $\ddot{c} = 0$.

There is a time t_C (Fig. 29) when the shock between regions 1 and 2 crosses the first I-characteristic. In its vicinity, if no special provisions are taken, the time step would decrease indefinitely since it is proportional to the physical mesh size and this in turn decreases indefinitely, when the region 2 is squeezed between the shock and the first characteristic (the number of mesh points remaining constant). Therefore, once the width of

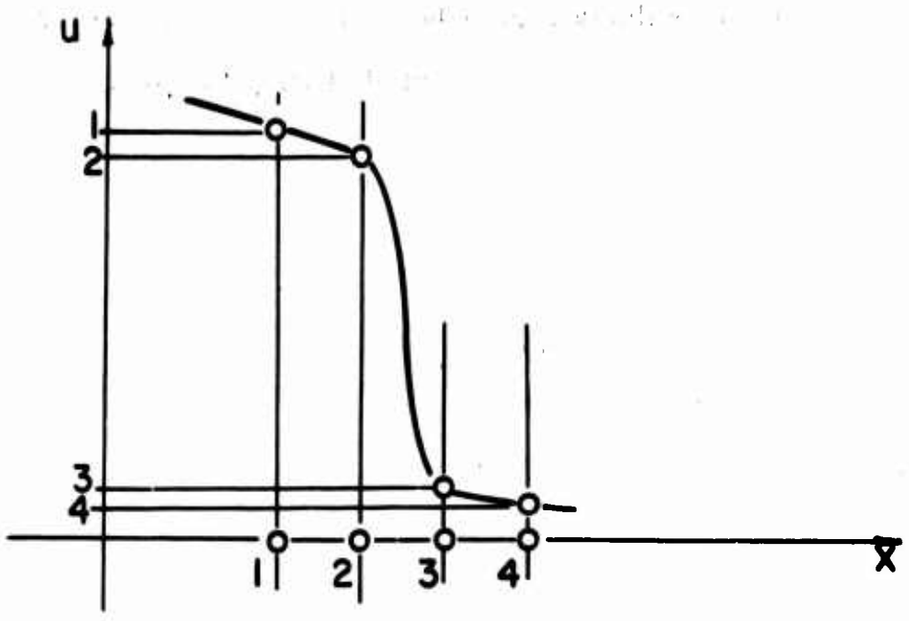

FIG. 30 BEHAVIOR OF u(x) IN THE NEIGHBORHOOD OF AN INCIPIENT SHOCK

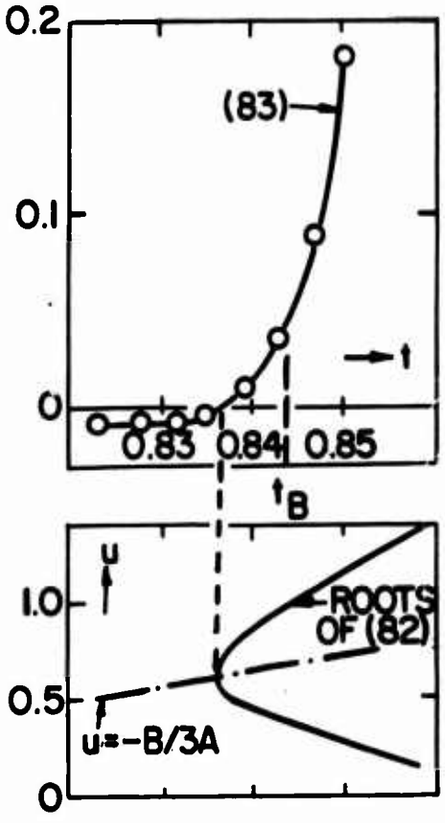

FIG. 31

region 2 becomes less thana prescribed value, the computation of the region is dropped and only region 1 is computed, letting the shock divide it from the gas at rest.

3.5. Prediction of the formation of a shock.

At $t = t_C$, one of the two regions disappears. The inverse situation arises at $t = t_B$, and it is a much more difficult one. Prior to t_B, the computation proceeds as described in Section 2.3. We need a criterion to detect the origin of a shock, and the criterion must furnish the location of point B, in space and time, to within one mesh interval in space and one or two steps in time, lest wiggles appear. This is indeed a very difficult problem in that a point must be found where u_x becomes infinite, when we only dispose of a discreet number of values of u. Obviously, no finite difference approximation to a derivative can ever become infinite and any identification of infinity with "a very large value" is arbitrary. A study of the flow in the vicinity of point B (Fig. 19) should guide us to find a better criterion.

Let us consider the mesh interval where the slope of u(x) is the highest and four nodes (in the computational space), two at the left and two at the right of it (Fig. 30). Since we are interested in a situation where u_x becomes infinite, it is better to consider x as a function of u rather than u as a function of x.

The simplest polynomial having a chance of giving a fair approximation to x(u) in the interval shown in the figure is a third order polynomial:

$$x = A\,u^3 + B\,u^2 + C\,u + D \tag{81}$$

We are looking for the case where the condition

$$\frac{dx}{du} = 3\,A\,u^2 + 2\,B\,u + C = 0 \tag{82}$$

is satisfied by one real value of u. This requires

$$B^2 - 3AC = 0 \qquad (83)$$

Suppose now that A, B, and C are determined to fit the values of x(u) at the four points of Fig. 30. We can use (83) as a test. In the simple wave, $B^2 - 3AC$ should generally be negative since no real value of u satisfies (82). When t_B is reached, $B^2 - 3AC$ should vanish and then become positive, and this yields a possible criterion for the detection of t_B. If x_1 is the value of x at point 1, the values of x at points 2, 3, and 4 are $x_1 + \Delta x$, $x_1 + 2\Delta x$, $x_1 + 3\Delta x$. By writing (81) for these four points, and calling δ the determinant of the coefficients of the right hand sides, we obtain

$$A = \frac{\Delta x}{\delta}\begin{vmatrix} 0 & u_1^2 & u_1 & 1 \\ 1 & u_2^2 & u_2 & 1 \\ 2 & u_3^2 & u_3 & 1 \\ 3 & u_4^2 & u_4 & 1 \end{vmatrix} = -\frac{\Delta x}{\delta}\begin{vmatrix} u_3^2 - 2u_2^2 + u_1^2 & u_3 - 2u_2 + u_1 \\ u_4^2 - 2u_3^2 + u_2^2 & u_4 - 2u_3 + u_2 \end{vmatrix} = -\frac{\Delta x}{\delta} f(2,1)$$

and, similarly,

$$B = \frac{\Delta x}{\delta} f(3,1) \ , \quad C = -\frac{\Delta x}{\delta} f(3,2)$$

Therefore the criterion suggested by (83) can be written as

$$\left[f(3,1)\right]^2 - 3\, f(3,2)\, f(2,1) \leq 0 \qquad (84)$$

Fig. 31 shows the trend of the left hand side of (84) in the calculation of Fig. 19.

Finally, Fig. 32 shows plots of u(x) at different times for a calculation of the problem of section 2.3 carried along indefinitely beyond t_B. The criterion above to determine t_B is applied, then the computational region is split into two parts; at t_C the second region is dropped again, as described above. The coding of this program is not shown since it can be easily obtained as an extension of Appendix 3. All simple arrays should in this case

be double arrays, to permit values of the physical parameters in different regions to be distinguished from each other; similarly, quantities such as b, c, b, Δx etc., should be stored in arrays, one value for each region. More details on the treatment of a problem with multiple shocks, including the problem above as a particular case, will be found in another paper.

Acknowledgements

Working on the present paper has been made more enjoyable by countless exciting discussions with colleagues at Polytechnic Institute of Brooklyn, several other Universities, and industrial establishments to all of whom I am very grateful. I would like to give here special thanks to Dean Martin H. Bloom, PIB, and to Gianky da Forno and Michael Abbett of General Applied Science Laboratories, Westbury, N. Y.

References

1. Moretti, G.: The Choice of a Time-Dependent Technique in Gas Dynamics. Polytechnic Institute of Brooklyn, PIBAL Report No. 69-26, 1969.

2. von Neumann, J. and Richtmyer, R.D.: A Method for the Numerical Calculation of Hydrodynamic Shocks. J. Appl. Phys. 21, pp. 232-237, 1950. Reprinted in AIAA Selected Reprint Series, Vol. IV, Computational Fluid Dynamics (C.K. Chu, Ed.), 1969.

3. Lax, P.: Weak Solutions of Nonlinear Hyperbolic Equations and Their Numerical Computation. Comm. Pure and Appl. Math., VII, pp. 159-193, 1954.

4. Emery, A.F.: An Evaluation of Several Differencing Methods for Inviscid Fluid Flow Problems. J. Comp. Phys., 2, pp. 306-331, 1968.

5. Lax, P. and Wendroff, B.: Systems of Conservation Laws. Comm. Pure and Appl. Math., XIII, pp. 217-237, 1960.

6. Richtmyer, R.D. and Morton, K.W.: Difference Methods for Initial-Value Problems. Second Edition, Interscience Publ., New York, 1967.

7. Moretti, G. and Salas, M.D.: Numerical Analysis of Viscous One-Dimensional Flows. Polytechnic Institute of Brooklyn, PIBAL Report No. 69-27, 1969.

8. Boericke, R.R.: A Numerical Investigation of Lax and Lax-Wendroff Difference Schemes Applied to Multi-dimensional Unsteady Flows. General Electric Co., Report TI67SD357, 1967.

9. Courant, R. and Friedrichs, K.O.: Supersonic Flow and Shock Waves. Interscience Publ., New York, 1948.

10. Courant, R., Friedrichs, K.O., and Lewy, H.: Ueber die Partiellen Differenzgleichungen der Mathematischen Physik. Math. Ann., 100, pp. 32-74, 1928.

11. Crocco, L.: A Suggestion for the Numerical Solution of the Steady Navier-Stokes Equations. AIAA J., 3, pp. 1824-1832, 1965.

APPENDIX I

```
      DIMENSION R(50),Q(50),E(50),QR(50),QM(50),HR(50),HM(50),HE(50),RN
     1(50),EN(50),U(50),H(50)
      REAL M(50),MN(50)
      DATA SIG,P2,R2,E1,Q1,QE/.1,4.5,2.66666666666667,5.3,6.6,.4/
  100 FORMAT(1H0/(10E12.4))
  101 FORMAT(1H1/I10)
      SIG2=SIG**2          $ GF=SQRT(1.4)          $ U1=-2.*GF
      U2=U1/R2             $ E2=2.5*P2+1.05        $ H1=-12.6*GF
      DO1 N=1,20           $ E(N)=E2               $ U(N)=U2
    1 R(N)=R2
      DO 2 N=21,40         $ E(N)=E1               $ U(N)=U1
    2 R(N)=1.
      DO 3 N=1,40          $ M(N)=U1               $ Q(N)=Q1
    3 H(N)=H1
      U(21)=U1+.0001
      M(21)=U(21)
      Q(21)=.4*E(21)+.8*U(21)**2
      H(21)=U(21)*(1.4*E(21)-.2*U(21)**2)
      K=0
    8 K=K+1
      IF(FLOAT(K/10).NE.FLOAT(K)/10.)GO TO 7
      WRITE(6,101)K
      WRITE(6,100)(U(N),N=1,40)
      WRITE(6,100)(M(N),N=1,40)
      WRITE(6,100)(Q(N),N=1,40)
    7 IF(K.GT.200)CALL EXIT
      DO 4 N=1,40
      QR(N)=-.8*U(N)**2
      QM(N)=1.6*U(N)
      HR(N)=-1.4*U(N)*E(N)/R(N)+.4*U(N)**3
      HM(N)=1.4*E(N)/R(N)-.6*U(N)**2
    4 HE(N)=1.4*Q(N)
      DO 5 N=2,39
      DMP=M(N+1)-M(N)      $ DQP=Q(N+1)-Q(N)       $ DHP=H(N+1)-H(N)
      DMM=M(N)-M(N-1)      $ DQM=Q(N)-Q(N-1)       $ DHM=H(N)-H(N-1)
      RN(N)=R(N)-(DMP+DMM)*SIG+2.*(DQP-DQM)*SIG2
      MN(N)=M(N)-(DQP+DQM)*SIG+((QR(N+1)+QR(N))*DMP+(QR(N)+QR(N-1))*DMM+
     1(QM(N+1)+QM(N))*DQP+(QM(N)+QM(N-1))*DQM+2.*QE*(DHP+DHM))*SIG2
      EN(N)=E(N)-(DHP+DHM)*SIG+((HR(N+1)+HR(N))*DMP+(HR(N)+HR(N-1))*DMM+
     1(HM(N+1)+HM(N))*DQP+(HM(N)+HM(N-1))*DQM+(HE(N+1)+HE(N))*DHP+(HE(N)
     2+HE(N-1))*DHM)*SIG2
      IF(ABS(RN(N)-R(N)).LT.1.E-9) RN(N)=R(N)
      IF(ABS(MN(N)-M(N)).LT.1.E-9) MN(N)=M(N)
      IF(ABS(EN(N)-E(N)).LT.1.E-9) EN(N)=E(N)
    5 CONTINUE
      DO 6 N=2,39          $ R(N)=RN(N)            $ M(N)=MN(N)
      E(N)=EN(N)           $ U(N)=M(N)/R(N)        $ Q(N)=.4*E(N)+.8*U(N)*M(N)
    6 H(N)=U(N)*(1.4*E(N)-.2*U(N)*M(N))
      GO TO 8
      END
```

APPENDIX II

```
      COMMON K,NA,NC,GAMMA,X0,TEND,GA,GD,GF,TIME,DT,DT2,DX,DDX,DDX2,BSEC
     1,X(100),XX(100),P(100),U(100),A(100),T(100),S(100),SN(100),UN(100)
     2,PN(100)
      DATA/X/1000*0./

  100 FORMAT(8E10.4)
  101 FORMAT(1H1,4E15.4)

      READ(5,100)GAMMA,X0,AN,TEND
      WRITE(6,101)GAMMA,X0,AN,TEND
      GA=GAMMA/(GAMMA-1.)
      GD=.5*(GAMMA-1.)
      GF=SQRT(GAMMA)
      DX=X0/AN
      NA=AN
      DDX=.5/DX
      DDX2=1./DX/DX
      NC=NA+1
      DO 2 N=1,NC
      X(N)=DX*FLOAT(N-1)
      XX(N)=X(N)
      A(N)=GF
    2 T(N)=1.
      K=1
      TIME=0.
C
    3 K=K+1
      DT=100.
      DO 7 N=1,NC
      DT1=.7*DX/(U(N)+A(N))
      IF(DT1.GT.DT)GO TO 7
      DT=DT1
    7 CONTINUE
      TIME=TIME+DT
      DT2=DT**2/2.
      CALL PISTON
      A1=GF+GD*UN(1)
      PN(1)=GA*ALOG(A1**2/GAMMA)
      CALL POINTS
      DO 8 N=1,NC
      XX(N)=XX(1)+X(N)
      U(N)=UN(N)
      S(N)=SN(N)
      P(N)=PN(N)
      T(N)=EXP(P(N)/GA+S(N)/GAMMA)
      A(N)=GF*SQRT(T(N))
    8 CONTINUE
      CALL OUTPUT
      IF(TIME.LE.TEND)GO TO 3
      CALL EXIT
      END
```

```
      SUBROUTINE POINTS
      DO 1 N=2,NA
      UX=(U(N+1)-U(N-1))*DDX
      PX=(P(N+1)-P(N-1))*DDX
      SX=(S(N+1)-S(N-1))*DDX
      TX=T(N)*(PX/GA+SX/GAMMA)
      UXX=(U(N+1)+U(N-1)-2.*U(N))*DDX2
      PXX=(P(N+1)+P(N-1)-2.*P(N))*DDX2
      SXX=(S(N+1)+S(N-1)-2.*S(N))*DDX2
      AC=U(N)-U(1)
      PT=-(AC*PX-GAMMA*UX)
      UT=-(AC*UX+T(N)*PX)
      ST=-AC*SX
      TT=T(N)*(PT/GA+ST/GAMMA)
      ACX=UX
      ACT=UT-BSEC
      PTX=-(ACX*PX+AC*PXX+GAMMA*UXX)
      UTX=-(ACX*UX+AC*UXX+TX*PX+T(N)*PXX)
      STX=-(ACX*SX+AC*SXX)
      PTT=-(ACT*PX+AC*PTX+GAMMA*UTX)
      UTT=-(ACT*UX+AC*UTX+TT*PX+T(N)*PTX)
      STT=-(ACT*SX+AC*STX)
      PN(N)=P(N)+PT*DT+PTT*DT2
      UN(N)=U(N)+UT*DT+UTT*DT2
      SN(N)=S(N)+ST*DT+STT*DT2
    1 CONTINUE
      RETURN
      END
```

APPENDIX III

```
      COMMON K,NA,NC,GAMMA,X0,TEND,GA,GB,GC,GD,GE,GF,TIME,DT,DT2,D,DX,
     1DDX,DDX2,B,C,BDOT,CDOT,BSEC,CSEC,XA,X(100),XX(100),P(100),U(100),
     2A(100),T(100),S(100),PN(100),UN(100),SN(100)
C
  100 FORMAT(8E10.4)
  101 FORMAT(1H1,4E15.4)
C
      READ(5,100)GAMMA,X0,AN,TEND
      WRITE(6,101)GAMMA,X0,AN,TEND
      GA=GAMMA/(GAMMA-1.)
      GB=1./(GAMMA-1.)
      GC=(GAMMA+1.)*GB
      GD=.5*(GAMMA-1.)
      GE=.5*(GAMMA+1.)
      GF=SQRT(GAMMA)
      NA=AN
      NC=NA+1
      TIME=.01
      CALL PISTON
      B=XX(1)
      U(1)=UN(1)
      XX(NC)=GF*TIME
      DX=1./AN
      D=XX(NC)-XX(1)
      DDX=.5/DX
      DDX2=1./DX/DX
      DO 2 N=1,NC
      X(N)=DX*FLOAT(N-1)
      XX(N)=X(N)*D+XX(1)
      U(N)=U(1)*(1.-X(N))
      P(N)=2.*GA*ALOG(1.+U(N)*GD/GF)
      S(N)=0.
      A(N)=GF+GD*U(N)
    2 T(N)=A(N)**2/GAMMA
      C=XX(NC)
      CDOT=GF
      CSEC=0.
      K=1
    3 K=K+1
      DT=100.
      DO 7 N=1,NC
      DT1=.7*DX/(U(N)+A(N))*D
      IF(DT1.GT.DT)GO TO 7
      DT=DT1
    7 CONTINUE
      TIME=TIME+DT
      DT2=DT**2/2.
      CALL PISTON
      A1=GF+GD*UN(1)
      PN(1)=GA*ALOG(A1**2/GAMMA)
      SN(1)=0.
      CALL POINTS
      CALL SHOCK
      B=XX(1)
      BDOT=UN(1)
      D=C-B
      DO 8 N=1,NC
      XX(N)=B+X(N)*D
      U(N)=UN(N)
      P(N)=PN(N)
      S(N)=SN(N)
      T(N)=EXP(P(N)/GA+S(N)/GAMMA)
      A(N)=GF*SQRT(T(N))
    8 CONTINUE
      CALL OUTPUT
      IF(TIME.LE.TEND)GO TO 3
      CALL EXIT
      END
```

APPENDIX III (con't.)

```
      SUBROUTINE POINTS
      DO 1 N=2,NA
      AA=1./D
      UX=(U(N+1)-U(N-1))*DDX
      PX=(P(N+1)-P(N-1))*DDX
      SX=(S(N+1)-S(N-1))*DDX
      TX=T(N)*(PX/GA+SX/GAMMA)
      UXX=(U(N+1)+U(N-1)-2.*U(N))*DDX2
      PXX=(P(N+1)+P(N-1)-2.*P(N))*DDX2
      SXX=(S(N+1)+S(N-1)-2.*S(N))*DDX2
      AC=AA*((X(N)-1.)*BDOT-X(N)*CDOT+U(N)
      AD=GAMMA*AA
      AE=AA*T(N)
      PT=-(AC*PX+AD*UX)
      UT=-(AC*UX+AE*PX)
      ST=-AC*SX
      TT=T(N)*(PT/GA+ST/GAMMA)
      ACX=AA*(BDOT-CDOT+UX)
      AEX=AA*TX
      PTX=-(ACX*PX+AC*PXX+AD*UXX)
      UTX=-(ACX*UX+AC*UXX+AEX*PX+AE*PXX)
      STX=-(ACX*SX+AC*SXX)
      AAT=-AA**2*(CDOT-BDOT)
      ACT=AAT*AC/AA+AA*((X(N)-1.)*BSEC-X(N)*CSEC+UT)
      ADT=GAMMA*AAT
      AET=AAT*T(N)+AA*TT
      PTT=-(ACT*PX+AC*PTX+ADT*UX+AD*UTX)
      UTT=-(ACT*UX+AC*UTX+AET*PX+AE*PTX)
      STT=-(ACT*SX+AC*STX)
      PN(N)=P(N)+PT*DT+PTT*DT2
      UN(N)=U(N)+UT*DT+UTT*DT2
      SN(N)=S(N)+ST*DT+STT*DT2
    1 CONTINUE
      RETURN
      END
```

APPENDIX III (con't.)

```
      SUBROUTINE SHOCK
      DIMENSION W(2),ERR(2)
  102 FORMAT(8HOFAILURE)
      C=CDOT*DT+C
      ME=1
      KIP=1
      W(1)=CDOT
      W(2)=1.0001*CDOT
      UN(NC)=U(NC)
      AN=A(NC)
      USTAR=U(NC)
      ASTAR=A(NC)
   60 EM2=W(ME)**2/GAMMA
      PS=(GAMMA*EM2-GD)/GE
      RS=(GC*PS+1.)/(GC+PS)
      XXSTAR=C-(UN(NC)+USTAR+AN+ASTAR)/2.*DT
      XSTAR=(XXSTAR-B)/D
      EPS=(XSTAR-X(NA))/DX+.5
      ASTAR=A(NA)+EPS*(A(NC)-A(NA-1))
      USTAR=U(NA)+EPS*(U(NC)-U(NA-1))
      PSTAR=P(NA)+EPS*(P(NC)-P(NA-1))
      UREL=-W(ME)/RS
      UN(NC)=UREL+W(ME)
      PN(NC)=PSTAR-GAMMA/ASTAR*(UN(NC)-USTAR)
      AN=SQRT(GAMMA*PS/RS)
      ERR(ME)PN(NC)-ALOG(PS)
      IF(ME.EQ.2)GO TO 62
      ME=2
      GO TO 60
   62 IF(ABS(ERR(ME)).LE.1.E-5)GO TO 61
      WA=W(1)-ERR(1)*(W(2)-W(1))/(ERR(2)-ERR(1))
      ERR(1)=ERR(2)
      W(1)=W(2)
      W(2)=WA
      KIP=KIP+1
      IF(KIP.LE.20)GO TO 60
      WRITE(6,102)
      CALL EXIT
   61 SN(NC)=PN(NC)-ALOG(RS)*GAMMA
      CSEC=(W(ME)-CDOT)/DT
      CDOT=W(ME)
      RETURN
      END
```

Unclassified
Security Classification

DOCUMENT CONTROL DATA · R & D

(Security classification of title, body of abstract and indexing annotation must be entered when the overall report is classified)

1. ORIGINATING ACTIVITY (Corporate author)	2a. REPORT SECURITY CLASSIFICATION
Polytechnic Institute of Brooklyn Dept. of Aerospace Engrg. and Applied Mechanics Route 110, Farmingdale, New York 11735	Unclassified
	2b. GROUP

3. REPORT TITLE

A CRITICAL ANALYSIS OF NUMERICAL TECHNIQUES: THE PISTON-DRIVEN INVISCID FLOW

4. DESCRIPTIVE NOTES (Type of report and inclusive dates)

Research Report

5. AUTHOR(S) (First name, middle initial, last name)

Gino Moretti

6. REPORT DATE	7a. TOTAL NO. OF PAGES	7b. NO. OF REFS
July 1969	68	11

8a. CONTRACT OR GRANT NO.	9a. ORIGINATOR'S REPORT NUMBER(S)
Nonr 839(38) b. PROJECT NO c. ARPA Order No. 529 d.	PIBAL REPORT NO. 69-25 9b. OTHER REPORT NO(S) (Any other numbers that may be assigned this report)

10. DISTRIBUTION STATEMENT

Distribution of this document unlimited.

11. SUPPLEMENTARY NOTES	12. SPONSORING MILITARY ACTIVITY
	Office of Naval Research Electronics Branch Washington, D.C.

13. ABSTRACT

This paper consists of two parts. In the first, a critical analysis of well-known procedures for the computation of one-dimensional shocked flows is made, in order to show the inconveniences of computing finite differences across a discontinuity and to prove that the use of the equations of motion in conservation form does not make the results any more accurate. In the second, a technique is developed to treat one-dimensional inviscid problems and it is applied to the problem of an accelerating piston. Practical and safe ways to predict the formation of a shock and to follow it up in its evolution are given.

DD FORM 1 NOV 65 1473

Unclassified
Security Classification